Title

Transcriptomic characterization of signaling pathways associated with osteoblastic differentiation of MC-3T3E1 cells

Short Title

Pathways analysis of osteoblast differentiation

Authors

Louis M. Luttrell[1,2,3*], Moahad S. Dar[4], Diane Gesty-Palmer[4], Hesham M. El-Shewy[1], Katherine M. Robinson[1], Courtney J. Haycraft[5], Jeremy L. Barth[6]

Affiliations

[1] Department of Medicine, Medical University of South Carolina, Charleston, SC, USA

[2] Department of Biochemistry & Molecular Biology, Medical University of South Carolina, Charleston, SC, USA

[3] Ralph H. Johnson Veterans Affairs Medical Center, Charleston, SC, USA

[4] Department of Medicine, Duke University Medical Center, Durham, NC, USA

[5] Department of Biology, Mississippi College, Clinton, MS, USA

[6] Department of Regenerative Medicine and Cell Biology, Medical University of South Carolina, Charleston, SC, USA

* Corresponding Author

E-mail: luttrell@musc.edu (LML)

Abstract

Bone remodeling involves the coordinated actions of osteoclasts, which resorb the calcified bony matrix, and osteoblasts, which refill erosion pits created by osteoclasts to restore skeletal integrity and adapt to changes in mechanical load. Osteoblasts are derived from pluripotent mesenchymal stem cell precursors, which undergo differentiation under the influence of a host of local and environmental cues. To characterize the autocrine/paracrine signaling networks associated with osteoblast maturation and function, we performed gene network analysis using complementary "agnostic" DNA microarray and "targeted" NanoString™ nCounter datasets derived from murine MC3T3-E1 cells induced to undergo synchronized osteoblastic differentiation *in vitro*. Pairwise datasets representing changes in gene expression associated with growth arrest (day 2 to 5 in culture), differentiation (day 5 to 10 in culture), and osteoblast maturation (day 10 to 28 in culture) were analyzed using Ingenuity Systems™ Pathways Analysis to generate predictions about signaling pathway activity based on the temporal sequence of changes in target gene expression. Our data indicate that some pathways known to be involved in osteoblast differentiation, e.g. Wnt/β-catenin signaling, are most active early in the process, while others, e.g. TGFβ/BMP, cytokine/JAK-STAT and TNFα/RANKL signaling, increase in activity as differentiation progresses. Collectively, these pathways contribute to the sequential expression of genes involved in the synthesis and mineralization of extracellular matrix. These results provide insight into the temporal coordination and complex interplay between signaling networks controlling gene expression during osteoblast differentiation. A more complete understanding of these processes may aid the discovery of novel

44 methods to promote osteoblast development for the treatment of conditions characterized
45 by low bone mineral density.

46 Introduction

47 Bone remodeling is the continuous process through which worn bone is removed
48 and replaced [1, 2]. Bone-resorbing osteoclasts differentiate from hematopoietic stem
49 cell precursors in response to cues originating from osteocytes, bone lining cells, and
50 differentiating osteoblasts. Bone-forming osteoblasts derive from mesenchymal stem cell
51 presursors and undergo a defined maturational sequence from proliferating preosteoblasts
52 to mature synthetically active osteoblasts, before finally undergoing apoptosis or
53 transforming into osteocytes embedded within the bony matrix and quiescent bone lining
54 cells covering the mineralized surface. The bone remodeling cycle involves sequential
55 osteoclastic bone resorption followed by the synthesis and mineralization of new bone
56 matrix by osteoblasts, a process that requires several weeks to complete. Since these
57 osteoclast-osteoblast bone forming units that mediate this process are constantly being
58 created and destroyed, any analysis performed on bone tissue, whether by classical
59 histomorphometry or using genomic and proteomic methods, is a ‘snapshot’ of the
60 metabolic state of bone at that moment in time. While such *in vivo* studies are extremely
61 useful for understanding the effects of disease, hormone administration/withdrawal or
62 drug treatment on overall bone metabolism, they inevitably capture cross sectional data
63 from multiple cell types in different differentiation states.

64 In contrast, *in vitro* studies offer the advantage that cellular development can be
65 synchronized, offering a better opportunity to view differentiation as a linear process. In
66 bone, the replication of undifferentiated osteogenic precursor cells, their recruitment to

remodeling bone matrix, and their subsequent acquisition of differentiated function, results from the complex interplay of signals transmitted by mechanical load, polypeptide growth factors, steroid and thyroid hormones, and locally produced cytokines and prostaglandins [3, 4]. While circulating hormones play an important modulatory role, osteoblastic differentiation can be induced *in vitro*, indicating that, once triggered, the process is autonomous, i.e. independent of ongoing exposure to systemically derived factors.

Gene array technology is a potentially powerful tool for understanding complex biological processes. A significant limitation of the approach, however, is that it is difficult to translate lists of significantly regulated genes into changes in biologically relevant signaling networks. Genomic datasets are invariably incomplete and contain some number of false positive 'hits', making candidate based follow up studies unreliable. In addition, important pathway components may not be regulated at the transcriptional level. Circumventing these limitations requires the use of bioinformatic approaches that compare changes in gene expression against databases of known protein-protein interactions to establish the probability that a given signaling or metabolic pathway is regulated under varying experimental conditions [5, 6]. These *in silico* analyses, which enable gene expression profile data to be expressed as the statistical probability that a particular pathway is regulated, can "fill in the blanks", leading to a more holistic view of process-related changes in signaling pathway activity.

To better understand the temporal regulation of osteoblast differentiation, we performed microarray analysis of gene expression followed by signal transduction pathways analysis on murine MC3T3-E1 cells undergoing osteoblastic differentiation *in*

vitro. Taking advantage of their well-defined maturational sequence [7-10], we isolated RNA at four stages: during log growth, early and late osteoblastic differentiation, and mature synthetic function. We then performed pairwise comparisons to identify significant changes in gene expression associated with each of these stages of osteoblast development, and used the resulting genesets to identify the time-dependent changes in signal transduction pathway activity. Our data indicate that the temporally coordinated activation of signaling pathways known to be involved in osteoblast differentiation, e.g. Wnt/β-catenin, Transforming Growth Factor-β (TGFβ) Bone Morphogenic Protein (BMP), cytokine/Janus Kinase (JAK)-Signal Transducer and Activator of Transcription (STAT), and Tumor Necrosis factor-α (TNFα□/Receptor Activator of Nuclear Factor κ-B (NFκB) Ligand (RANKL) signaling, correlates with the sequential expression of genes involved in the biosynthesis and mineralization of extracellular matrix as differentiation progresses. These results demonstrate the utility of functional genomic approaches to microarray analysis and offer insight into the temporal sequence of changes in the autocrine/paracrine signaling networks regulating osteoblast differentiation.

Materials and methods

Culture and differentiation of MC3T3-E1 cells

Stock cultures of MC3T3-E1 cells (subclone 4; CRL-2593; ATCC) were maintained in α-minimum essential medium (MEM) supplemented with 10% v/v fetal bovine serum, penicillin (100 units/mL) and streptomycin (100 pg/mL) in a humidified 10% CO_2 atmosphere at 37 ˚C. Until the time of study cells were maintained in log phase growth by passage every 3-5 days using 0.001% pronase (w/v) to detach adherent cells. For studies of the temporal sequence of osteoblast differentiation, cells were plated at an

initial density of 20,000 cells/well in 6-well plates or 100,000 cells/dish in 10 cm dishes, and grown for 2 to 28 days in α-MEM supplemented with 10% v/v fetal bovine serum, 5 mM β-glycerol phosphate and 50 μg/mL ascorbic acid (7-10).

Cell replication

Between days 1 and 5 in culture, cells in 6-well plates were treated with 0.001% pronase (w/v) to achieve detachment and directly counted in a hemocytometer.

Alkaline phosphatase activity

Alkaline phosphatase activity was measured by para-nitrophenyl phosphate hydrolysis as previously described (11). Briefly, MC3T3-E1 cells growth in 6-well plates were harvested in distilled water and disrupted by sonication. Appropriately diluted aliquots of cell lysate containing equal cell protein were incubated for 30 min at 37 ˚C in a final reaction volume of 600 □L, containing 1.0 M diethanolamine, pH 10.3 and 15 mM para-nitrophenyl phosphate. Reactions were terminated by the addition of 2.4 mL 0.1N NaOH, after which generation of para-nitrophenol was measured by determining absorbance at 400 nm. Results were expressed as pmol para-nitrophenol/min/10^6 cells.

Synthesis of type I collagen

Type 1 collagen production was determined by western blotting. Monolayers of MC3T3-E1 cells were lysed directly in 1X Laemmli sample buffer, dispersed by sonication, and resolved by sodium dodecyl sulfate – polyacrylamide gel electrophoresis. Immune complexes on nitrocellulose membranes were detected using mouse monoclonal anti-type I collagen IgG_1 (COL1A: sc59772; Santa Cruz Biotechnology, Santa Cruz, CA) with horseradish peroxidase-conjugated donkey anti-mouse IgG (Code: 715-035-150;

Jackson ImmunoResearch Laboratories Inc., West Grove, PA) as secondary antibody. The cell content of each sample was determined by western blotting in parallel for α-actin using mouse monoclonal anti-actin IgG_1 (C-2: sc8432; Santa Cruz Biotechnology, Santa Cruz, CA). Immune complexes were visualized on X-ray film by enzyme-linked chemiluminescence and quantified using a Fluor-S MultiImager. Data were expressed as the ratio of type I collagen to α-actin in each sample.

Alizarin red staining

Matrix mineralization was quantified by Alizarin red staining as described (12). Monolayers of MC3T3-E1 cells in 6-well plates were fixed for 24 hr in a 10% formalin:methanol:distilled water solution (1:1:1.5), stained for 20 min in 2% Alizarin Red-S in distilled water, washed with distilled water and air dried. Mineralization was quantified by eluting the stain using 10% cetylpyridium chloride and measuring absorbance at 520 nM.

mRNA isolation

MC3T3-E1 cells were cultured as described in 10 cm dishes for 2, 5, 10 or 28 days prior to isolation of RNA. Total RNA from three independent cultures was isolated at each time point. Cells were harvested by scraping and RNA was isolated with Trizol Reagent (Invitrogen, Carlsbad, CA) and purified using the RNeasy kit (Qiagen Inc., Valencia, CA) according to the manufacturer's protocols (13). Total RNA was analyzed for concentration (ng/□L) and purity (ratios of 260/280 nm and 260/230 nm) using a NanoDrop 1000 Spectrophotometer (Thermo Scientific, Wilmington, DE). RNA integrity was analyzed using the Experion RNA HighSens Analysis Kit (Bio-Rad Laboratories Inc., Hercules CA).

158 # Microarray analysis

159 Samples underwent RNA amplification (Message Amp; Ambion, Austin, TX),
160 labeling with Cy3, and hybridization to Mouse Operon 17,000 gene feature (Operon
161 dataset; version 2.0) spotted oligonucleotide arrays in the microarray facility of the Duke
162 University Institute for Genome Sciences and Policy (*www.genome.duke.edu/cores/*
163 *microarray/*). MIAME compliant microarray data files have been deposited with the
164 NCBI GEO database (*www.ncbi.nlm.nih. gov/gds*) (GEO Series GSE64485). Data pre-
165 processing and normalization were performed on GenePix scan results files (.gpr files)
166 using the Bioconductor LimmaGUI package 1.28.0 run with R 2.13.0 software (14).
167 Background correction was performed using the normexp method with offset of 16, and
168 spot quality weighting was applied as follows: 1 for Good (100) or Unflagged (0); 0.1 for
169 Bad (-100), Not Found (-50) and Absent (-75) flags. Print-tip group loess normalization
170 was applied for normalization within arrays. Review of box plots of normalized M
171 values indicated that normalization between arrays was not warranted. Normalized M
172 values, i.e. log2 test(Cy3)/reference(Cy5) relationship, were imported into dchip for
173 comparative analysis. ANOVA was used to find genes differing as function of time, i.e.
174 significantly different between any two time points. ANOVA filtering at the 0.005 level
175 yielded 1005 genes passing with a reasonable 5-10% false discovery rate (17664
176 compared; expected false positive: 88). Self-organizing maps (SOM) were used to
177 partition the significantly regulated genes into different response patterns. Expression
178 data were imported into MeV software for SOM analysis, z-standardization performed,
179 i.e. mean=0 and SD=1, and SOM clusters for ANOVA $p<0.005$ were generated by: 16

clusters, 4x4, 2000 iterations, hexagonal topography, Gaussian neighborhood, alpha 0.05, radius 1.0, no HCL linkage, Pearson correlation.

NanoString™ nCounter analysis

The NanoString™ nCounter gene expression system (NanoString™ Technologies; Seattle, WA) was used for expression profiling of selected mRNA species isolated from MC3T3-E1 cells at Days 2, 5, 10 and 28 in culture using a custom nCounter CodeSet composed of 243 probes (S1 Table) including 6 housekeeping controls (Eif4a2, GusB, Oaz1, Stk36, Tceb1, and Tubb4a). With NanoString™ technology fluorescent single strand RNA probes are hybridized to complimentary target strands of mRNA and quantified based on the fluorescence of each target gene within each sample (15,16). Briefly, the NanoString™ reporter probe CodeSet was suspended in 70µL of hybridization buffer and 8µL aliquots were combined in sterile microfuge tubes with each RNA sample diluted to a concentration of 250ng RNA in 5µL. Thereafter, 2µL of the capture probe CodeSet was added to each tube, tubes were centrifuged, and then incubated at 65°C in a BioRad T100 Thermal Cycler (BioRad; Hercules, CA) for 13-15 hours. After hybridization, samples were analyzed using the NanoString™ Technologies Prep Station and Digitial Analyzer according to manufacturer's instructions. All 12 samples, i.e. RNA from triplicate cultures at each of four time points, were analyzed simultaneously to minimize batch effects. The resulting counts were analyzed using NanoStriDE and GraphPad Prism 7 (GraphPad Software; Carlsbad, CA) software. Statistical significance of change over time was determined by two-way ANOVA with Tukey's multiple comparisons test using GraphPad Prism 7.

IPA metabolic pathways analysis.

Network analysis of genesets representing changes in mRNA abuundance between specified time points was performed using the Ingenuity Systems™ Pathways Analysis (IPA) tool (Qiagen; Redwood City, CA). IPA compares Genbank Accession number/expression information with a proprietary protein-interaction database to establish the probability that a given signaling or metabolic pathway is activated under varying experimental conditions. For the microarray dataset, expression ratios for all relevant pairwise comparisions, i.e. D2 vs D5, D2 vs D10, D2 vs D28, D5 vs D10, D5 vs D28, and D10 vs D28, were calculated using the ANOVA $p<0.005$ set of 1005 significantly regulated genes. For the NanoString™ dataset, pairwise expression ratios were calculated for each of the 237 measurable genes. Expression ratio data were uploaded into the IPA Pathways Analysis system (*https://analysis.ingenuity.com/*), yielding 976 analyzable transcripts from the microarray dataset (S2 Table). Each dataset was subjected to IPA Core Analysis, then analyzed using IPA Upstream Regulator, Downstream Effects, and Canonical Pathways analytic tools. To capture pathway changes associated with each phase of differentiation we focused on the D2 vs D5, D5 vs D10, and D10 vs D28 pairwise comparisons. For IPA Upstream Regulator and Canonical Pathways analysis, gene clusters composed of ≥ 2 genes per group with $P < 0.05$ enrichment, i.e. $-\log(\text{p-value}) \geq 1.3$, compared with a standard murine background database were considered analyzable. The IPA output was exported as Microsoft Excel files to prepare the S3-7 Tables. Graphic representations of the data were prepared using either the IPA Canonical Pathways Molecular Activity Predictor tool or GraphPad Prism 7 software, as appropriate. To facilitate visual inspection of the changes in predicted Upstream Regulator and Canonical Pathways activity associated with each interval, heat

maps were generated from the activation z-scores using Morpheus software (*https://software.broadinstitute.org/morpheus/*).

Results

The temporal sequence of MC3T3-E1 cell differentiation

MC3T3-E1 cells undergo a well-characterized process of osteoblastic differentiation when placed in culture medium supplemented with β-glycerol phosphate and ascorbic acid [7-10]. Fig 1 presents this process tracked using traditional markers: cell number, bone alkaline phosphatase, abundance of type I collagen, and alizarin red staining. After initial seeding, the cells remain in log phase growth for 2-3 days, undergoing growth arrest upon attaining confluence by days 3-4. Osteoblastic differentiation begins upon growth arrest and continues through days 5 to 10 in culture, evident first as an increase in the production of bone-specific alkaline phosphatase, followed by deposition of a collagenous matrix composed in part of type 1 collagen. Matrix mineralization begins as early as day 10 and accelerates with time in culture. By day 28 the MC3T3-E1 derived osteoblasts have produced a mineralized matrix.

Fig 1. MC3T3-E1 osteoblast maturation *in vitro*. MC3T3-E1 cells were seeded in 6-well tissue culture plates at an initial density of 20,000 cells/well and maintained in culture for up to 28 days. **A.** Representative Alizarin Red stained culture dishes from Days 2, 5, 10 and 28 demonstrating the progression of matrix mineralization. **B.** Graph depicting change in cell number (days 1-5), secreted alkaline phosphatase activity (days 4-28), type 1 collagen synthesis (days 3-21), and matrix mineralization (days 4-28) associated with MC3T3-E1 differentiation. Data shown are the Mean ± SEM of triplicate

249 determinations. These data were used to select time points representing proliferating
250 preosteoblasts (day 2), early and late differentiating osteoblasts (days 5 and 10), and
251 active osteoblasts (day 28), for subsequent mRNA isolation.
252
253 Predictably, osteoblastic differentiation on MC3T3-E1 cells is reflected in
254 changes in the abundance of mRNA encoding bone marker proteins. As shown in Fig 2,
255 osteoblast developmental markers, matrix components, and proteins involved in cell
256 adhesion and matrix remodeling change over time as the cells evolve from proliferating
257 pre-osteoblasts to mature osteoblasts. Notably, these changes in mRNA abundance
258 appear at different times during development. mRNA encoding Runx2, the first
259 transcription factor required for determination of the osteoblast lineage [17,18], increases
260 early in development and plateaus between Days 5 and 10, while others, e.g. alkaline
261 phosphatase (*Alp1*), integrin-binding sialoprotein (*Ibsp*), a major structural protein of the
262 bone matrix, and parathyroid hormone receptor (*Pthr1*), increase steadily from Day 2 to
263 Day 28. Still other mRNA species are abundant throughout development, e.g. collagen
264 type 1A (*Col1a1*), and some increase between Days 10 and 28 after differentiation is well
265 underway e.g. the osteoblast-specific matrix protein periostin (*Postn*). Such differences
266 are consistent with a temporally coordinated process wherein early events trigger the
267 sequential activation of a transcriptional program driven by intracellular signaling
268 networks.
269
270 **Fig 2. Temporal changes in the abundance of mRNA encoding bone marker**
271 **proteins.** Total RNA was isolated from triplicate cultures of MC3T3-E1 cells at Days 2,

5, 10 and 28 in culture, and mRNA abundance quantified by NanoString nCounter using a bone focused probe set (S1 Table). Developmental markers shown are: alkaline phosphatase (*Alp1*); parathyroid hormone receptor (*Pthr1*); the transcription factors *Runx2*, *Sox9* and *Sp7*; and the transcriptional repressor *Msx2*. Matrix components shown are: bone gamma-carboxyglutamate protein (*Bglap*); collagen types 1A1 (*Col1a1*), 1A2 (*Col1a2*), 2A1 (*Col2a1*) and 10A1 (*Col10a1*); decorin (*Dcn*); dermatopontin (*Dpt*); dentin matrix protein-1 (*Dmp-1*); integrin-binding sialoprotein (*Ibsp*); and periostin (*Postn*). Proteins associated with cell adhesion and matrix remodeling are: tetraspanin (*Cd9*); cathepsin K (*Ctsk*); osteonectin (*Sparc*); osteopontin (*Spp1*); matrix metalloproteinases 2 (*Mmp2*), 14 (*Mmp14*), and 16 (*Mmp16*); hyaluronic acid receptor (*Cd44*); and neural cell adhesion molecule 1 (*Cd56*). Data shown represent the Mean ± SD of triplicate samples. Error bars not shown are smaller than the symbol. † $P < 0.05$; * $P < 0.01$; ** $P < 0.001$ different in abundance between at least two time points by two-way ANOVA with Tukey's multiple comparisons test; ns, not significant.

DNA microarray analysis of MC3T3-E1 differentiation

DNA microarrays, because they capture information about the abundance of a large number of unselected mRNA species, provide an "agnostic" snapshot of gene expression patterns at a given point in time. Combining microarray data on changes in mRNA abundance over time with bioinformatic tools, such as Ingenuity Systems™ IPA, provides a means to translate microarray data into a more complete picture of metabolic activity [5, 6]. To identify changes in gene expression occurring at different stages of differentiation, triplicate samples of total mRNA were isolated from subconfluent

MC3T3-E1 preosteoblasts (day 2), growth-arrested preosteoblasts (day 5), differentiating osteoblasts (day 10) and maturing synthetically-active osteoblasts (day 28), and hybridized to Operon V2.0 murine cDNA microarrays representing approximately 17,600 expressed sequence tags. Raw microarray data (GEO Series GSE64485) were analyzed by ANOVA to identify genes whose mean expression was significantly different between any two time points. Fig 3A shows a heat map of 1005 mRNAs passing the ANOVA filtered at $p < 0.005$. S2 Table lists the gene symbol, annotation, and observed abundance of the 976 analyzable mRNAs from this dataset. Hierarchical clustering revealed several distinct temporal patterns of expression, with some gene clusters increasing or decreasing in abundance early in differentiation, others changing progressively throughout differentiation, or changing most dramatically during the period of osteoblast maturation. Still others genes exhibited a biphasic pattern, increasing or decreasing with the onset of differentiation and reversing their direction of change between days 10 and 28 in culture. To further partition genes into different response patterns, we generated self-organizing maps (SOM) from the ANOVA $p<0.005$ dataset. As shown in Fig 3B, distinct temporal patterns of mRNA abundance were evident, reflecting each stage of osteoblast differentiation.

Fig 3. Temporal patterns of change in the MC3T3-E1 transcriptome during differentiation. Triplicate DNA microarrays at each time point were used to identify significantly regulated mRNAs at different phases of osteoblast differentiation by ANOVA ($p<0.005$; estimated false discovery rate 8.8%). **A.** Heat map representing observed mRNA abundance of 1005 genes identified by ANOVA as demonstrating a

318 significant difference between any two time points. Hierarchical clustering was used to
319 identify coordinated patterns of change. **B.** Sixteen cluster SOM representing temporal
320 changes in mRNA abundance associated with MC3T3-E1 differentiation. Expression
321 data were subjected to z-standardization and SOM assembled using MeV software. The
322 resulting 16 SOM clusters are shown grouped in relation to the differentiation state of
323 MC3T3-E1 cells. Growth arrest was associated with abrupt changes (increase or
324 decrease) in mRNA levels between days 2 and 5 (240 genes). The onset of differentiation
325 was associated with progressive changes in mRNA levels between days 2 and 10 (212
326 genes). Peak differentiation was associated with prominent changes in mRNA levels
327 between days 5 and 10 (246 genes). Osteoblast maturation was associated with prominent
328 changes in mRNA levels between days 10 and 28 (307 genes).
329
330 To test the hypothesis that the biological processes underlying osteoblastic
331 differentiation of MC3T3-E1 cells are reflected in the coordinated changes in the
332 transcriptome over time, the DNA microarray data were analyzed using Ingenuity
333 Systems™ IPA software. IPA compares empirically derived "omics" datasets, e.g. DNA
334 microarray data, with a curated database of reported gene-gene and protein-protein
335 interactions to predict signaling pathway activity based on observed changes in upstream
336 regulators and/or the downstream genes whose expression they control. The IPA output
337 includes two statistical measures. The first, which is typically expressed as –log(p-
338 value), represents the probability that the correlation between an input set of observed
339 factors and co-regulated genesets in the IPA database did not occur by chance. Hence, a
340 –log(p-value) greater than 1.3 represents $p < 0.05$ of a significant association. The

second, termed an activation z-score, is based on the degree to which observed changes in factor levels, e.g. increases or decreases in mRNA abundance between two points in time, correlate with the expected changes associated with pathway activation or inhibition. Thus, an activation z-score > 2 or < -2 predicts pathway activation or inhibition, respectively, with $p < 0.05$.

The biochemical characterization of differentiating MC3T3-E1 cells (Fig 1) demonstrates that the major downstream biological processes, e.g. cell proliferation versus matrix mineralization, change over time. To generate a gestalt view of whether the structure of the DNA microarray dataset reflects this temporal evolution, we calculated expression ratios for each of the 976 analyzable genes identified by ANOVA using three pairwise comparisons, day 2 to day 5 (D2 vs D5), day 5 to day 10 (D5 vs D10), and day 10 to day 28 (D10 vs D28), and performed IPA Downstream Effects Analysis, which predicts increases or decreases in downstream biological activities. S3 Table lists the annotation, -log(p-value), and activation z-score for all biological process terms identified from our dataset where the z-score was > 1 or < -1. These results are presented graphically in Fig 4. As shown, each pairwise comparison was associated with a set of unique of terms, here represented graphically as vertical bars. Importantly, terms identified in two overlapping comparisons exhibited a high degree of concordance in the predicted direction of activation/inhibition (20 of 26 terms appearing in both the D2 vs D5 and D5 vs D10 comparison, and 24 of 31 terms appearing in both the D5 vs D10 and the D10 vs D28 comparison). Consistent with the SOM analysis (Fig 3B), where some gene clusters increased in abundance steadily throughout differentiation, several process level terms were identified in all three genesets, and again there was strong concordance

364 in the predicted direction of activation/inhibition (20 of 23 terms appearing in all three
365 comparisons). Of interest, process terms appearing only in the D2 vs D5 and D10 vs D28
366 comparisons showed less concordance (only 9 of 29 terms were concordant). This too
367 may reflect at the process level expression patterns observed in the SOM analysis, where
368 some gene clusters clearly underwent reciprocal regulation, increasing/decreasing
369 between days 2 and 5, remaining relatively constant between days 5 and 10, and returning
370 to their prior levels between days 10 and 28.
371
372 **Fig 4. Temporal changes in mRNA abundance reflect evolving biological processes**
373 **during MC3T3-E1 differentiation.** The mRNA abundance of 976 significantly
374 regulated genes identified by ANOVA as changing during MC3T3-E1 differentiation was
375 used to calculate expression ratios comparing D2 vs D5, D5 vs D10, and D10 vs D28.
376 For each pairwise comparison, the earlier time point was used as the denominator and
377 later time point as the numerator, such that expression ratios reflect increases/decreases in
378 mRNA abundance as differentiation proceeds. IPA Downstream Effects Analysis was
379 performed to identify biological process terms associated with each interval and filtered
380 to include terms only with –log(p value) >1.3, minimum of two genes, and z-score >1 or
381 <-1. The graph depicts z-score values for terms associated with the period of growth
382 arrest and onset of differentiation (gold bars), active differentiation (blue bars), and
383 osteoblast maturation (lavender bars). The descriptive annotations associated with each
384 term are omitted for simplicity but presented in S3 Table.
385

386 To resolve the temporal changes in signaling networks associated with
387 osteoblastic differentiation of MC3T3-E1 cells we performed IPA Upstream Regulator
388 and Canonical Pathways Analysis using the 976 significantly regulated genes identified
389 by ANOVA. The IPA Upstream Regulator Analysis predicts which transcriptional
390 regulators are activated or inhibited based on observed changes in expression of
391 downstream genes. Predicted upstream regulators with activation Z-scores > 2 or < -2
392 during at least one phase of differentiation are shown in S4 Table. Individual upstream
393 regulators were grouped based on the signaling networks with which they are most
394 associated, and the z-scores derived from the D2 vs D5, D5 vs D10, and D10 vs D28
395 comparisons used to generate heat maps that illustrate the predicted change in regulator
396 activity as differentiation progresses. In these maps, rows represent individual upstream
397 regulators and columns represent time intervals. Predicted increases in activity from the
398 beginning to end of each interval, e.g. from day 2 to day 5, are indicated in red and
399 decreases in blue, with color intensity representing the magnitude of the z-score. Thus, an
400 upstream regulator that was predicted to increase in activity from day 2 to day 5, day 5 to
401 day 10, and day 10 to day 28 would be red in all columns, while one that increased from
402 day 2 to day 5 and then remained active at the same level would be red in the D2 vs D5
403 column, then white in the D5 vs D10 and D10 vs D28 columns. As shown in Fig 5A,
404 upstream regulators associated with cell cycle progression were predicted to become less
405 active over time, consistent with the growth arrest of MC3T3-E1 cells that heralds the
406 onset of differentiation. Conversely, upstream regulators of several pathways associated
407 osteoblast differentiation, e.g. TGFβ/BMP/SMAD, WNT/β-catenin, and Hedgehog

signaling [4] were predicted to become more active as differentiation progressed, as did regulators of TNFα/RANKL/NFκB and cytokine/JAK-STAT signaling.

Fig 5. Temporal changes in predicted upstream regulators and canonical signaling pathways associated with MC3T3-E1 cell differentiation. Microarray data on the 976 significantly regulated mRNA species were used to calculate change in expression ratio between D2 vs D5, D5 vs D10, and D10 vs D28. Expression ratios were analyzed using IPA Upstream Regulator and Canonical Pathways Analysis software and heat maps reflecting the changes in predicted activity during each interval were generated using Morpheus software. **A.** Heat maps depicting changes in selected upstream regulators (rows) with activation z-scores > 2 (red) or < -2 (blue) during at least one phase of differentiation (columns). Upstream regulators were arbitrarily grouped based on their involvement is biological processes or signaling pathways related to osteoblast differentiation. **B.** Heat maps depicting changes in z-score for selected canonical signaling pathways (rows) during each phase of differentiation (columns). Z-scores were subjected to Euclidean hierarchical clustering in Morpheus to group pathways based on similarity in temporal change.

To gain insight into how predicted changes in the activity of individual upstream regulators were integrated into signaling networks, we next performed IPA Canonical Pathways Analysis, which compares observed changes in mRNA abundance to the expected direction of change associated with pathway activation or inhibition. The list of signaling pathways represented in the dataset along with –log(p-value) and activation z-

score are shown in S5 Table. Fig 5B depicts a heat map of predicted changes in activity in selected canonical signaling pathways. Hierarchical clustering was performed to group pathways based on similarities in the change in activity over time. Considering pathways known to be involved in bone development, Wnt/β-catenin signaling decreased in activity as differentiation progressed, while TGFβ signaling increased. The TGF-β/BMP axis is a principal regulator of mesenchymal stem cell differentiation into cartilage and bone [19-22], acting through several effectors including SMADs, p38 mitogen-activated protein kinase (MAPK), and phosphatidyl inositol 3-kinase (PI3K)/AKT. TGF-β/BMP engages in extensive cross talk with other receptor-mediated signaling in bone, including WNT/β-catenin, Notch, Hedgehog, fibroblast growth factor (FGF), parathyroid hormone-related peptide (PTHrp), and interleukin (IL)/TNFα/interferon-γ cytokines that collectively signal via the JAK/STAT and NFκB pathways [4,23]. Notably, several of these pathways, e.g. p38 MAPK, STAT3, NFκB and IL6 signaling also showed a trend toward activation during differentiation.

NanoString™ analysis of MC3T3-E1 differentiation

To validate our "agnostic" microarray data on signaling pathway activation, we performed a "focused" analysis of MC3T3-E1 cell gene rexpression using NanoString™ nCounter. The NanoString™ nCounter system uses color-coded molecular "barcodes" attached target-specific probes to count up to several hundred unique transcripts in a single hybridization reaction [15,16]. The culture protocol used for the microarray experiment was repeated to provide independent mRNA samples. Triplicate samples of total mRNA isolated from MC3T3-E1 cells at days 2, 5, 10 and 28 in culture were

454 analyzed using a NanoString™ Code Set designed to quantify the abundance of 237
455 transcripts related to bone development and signaling. S1 Table lists the gene name,
456 annotation, and expression data for the NanoString™ probes. Fig 6A shows a heat map of
457 all 237 transcripts assayed. As with the microarray data, hierarchical clustering revealed
458 several distinct temporal patterns of expression, with some groups of transcripts
459 increasing/decreasing in abundance early in differentiation and others changing most
460 dramatically later during osteoblast maturation. Fig 6B-E shows temporal changes in
461 selected transcripts related to pathways identified in the bioinformatics analysis of the
462 microarray data. Significant changes in mRNA abundance were detected in ligands,
463 receptors or modulators of BMP, TGFβ and Activin signaling, the three closely-related
464 components of the TGFβ network, as well as in the TNFα-NFκB, interleukin-JAK/STAT,
465 and WNT/β-catenin pathways.
466
467 **Fig. 6. NanoString™ analysis of bone-related mRNAs during MC3T3-E1 cell**
468 **differentiation.** Total RNA was isolated from triplicate cultures of MC3T3-E1 cells at
469 days 2, 5, 10 and 28, and mRNA abundance quantified by NanoString™ nCounter using
470 a bone specific Code Set (S1 Table). **A.** Heat map depicting changes in mRNA
471 abundance for individual mRNA species (rows) over time in culture (columns) for day 2
472 (D2), day 5 (D5), day 10 (D10), and day 28 (D28). Expression data, after log2
473 adjustment, were subjected to Euclidean heirarchical clustering in Morpheus to group
474 genes based on similarity in temporal change. **B.** mRNA abundance of selected ligands,
475 receptors, modulators, and mediators related to BMP/TGFβ/Activin, TNFα/NFκB,
476 IL/JAK-STAT, and WNT/β-catenin signaling. BMP pathway components shown are:

BMP 4 (*Bmp4*); BMP receptor 1A (*Bmpr1a*); BMP receptor 2 (*Bmpr2*); the BMP co-receptors, repulsive guidance molecule (RGM) A (*Rgma*) and RGM B (*Rgmb*); the BMP negative regulators, Chordin and Noggin; and the DAN family BMP antagonist, Gremlin. TGFβ pathway components shown are: TGFβ1 (*Tgfb1*); TGFβ2 (*Tgfb2*); TGFβ3 (*Tgfb3*); TGFβ receptor 1 (*Tgfbr1*); and TGFβ receptor 2 (*Tgfbr2*). Activin pathway components shown are: inhibin subunit βA (*Inhba*); activin A receptor type 1 (*Acvr1*); activin A receptor type 1B (*Acvr1b*); activin A receptor type 2A (*Acvr2a*); BMP and activin membrane bound inhibitor (*Bambi*); and the activin and TGFβ receptor ligand, left-right determination factor 1 (*Lefty*). TNFα pathway components shown are: TNF ligand superfamily member 13-like (*April*); TNF (*Tnf*); RANKL (*Tnfsf11*); TNF-receptor superfamily member 4 (*Tnfrsf4*); receptor activator of NFκB (*Tnfrsf11a*); TNF receptor superfamily member 11b (*Tnfrsf11b*); and NFκB (*Nfkb*). Interleukin pathway components shown are: IL1B (*Il1b*); IL4 (*Il4*); IL7 (*Il7*); IL12A (*Il12a*); IL1 receptor-like 1 (*Il1rl1*); IL2 receptor β subunit (*Il2rb*); IL4 receptor α subunit (*Il4ra*); IL15 receptor α subunit (*Il15ra*); and STAT1 (*Stat1*). WNT pathway components shown are: WNT 5A (*Wnt5a*); Wnt 7A (*Wnt7a*); the WNT signaling pathway inhibitor, Dickkopf (*Dkk1*); β-catenin (*Ctnnb1*); the regulator of β-catenin stability, Axin 2 (*Axin2*); and the β-catenin regulated transcription factors, nuclear factor of activated T cells 1 (*Nfatc1*) and transcription factor 7 (*Tcf7*). In each graph, symbols representing ligands are show in green, receptor subunits in blue, intracellular mediators and modulators in red, and transcription factors in lavender. Data shown represent the Mean ± SD of triplicate samples. Error bars not shown are smaller than the symbol. † $P<0.05$; * $P<0.01$; **

499 P<0.001 different in abundance between at least two time points by two-way ANOVA
500 with Tukey's multiple comparisons test; ns, not significant.
501
502 To determine how the changing levels of pathway components translated into
503 changes in pathway activity during differentiation, we performed IPA Upstream
504 Regulator and Canonical Pathways Analysis using expression ratios derived from
505 comparisons of the NanoString™ data for D2 vs D5, D5 vs D10, and D10 vs D28.
506 Predicted upstream regulators with activation z-scores > 2 or < -2 during at least one
507 phase of differentiation are shown in S6 Table. Selected upstream regulators were
508 grouped based on the signaling networks with which they are most associated, and the z-
509 scores used to generate heat maps. As shown in Fig 7A, upstream regulator activity
510 associated with cell cycle progression, apoptosis, and cell survival tended to decrease
511 between days 2 and 5 and days 5 and 10, then increase between days 10 and 28. Notably,
512 activity of the anti-apoptotic regulators AKT1 and p38 MAPK that function downstream
513 of TGFβ/BMP and TNFα/RANKL increased as differentiation progressed. Coincident
514 with this, upstream regulators related to TGFβ/BMP/SMAD, WNT/β-catenin, and
515 Hedgehog signaling showed activation during osteoblastic differentiation, as did
516 regulators involved in TNFα/RANKL/NFκB, cytokine/JAK-STAT, receptor tyrosine
517 kinase (RTK), and G protein-coupled receptor (GPCR) signaling.
518
519 **Fig 7. Upstream regulators and canonical signaling pathways analysis of a focused**
520 **NanoString™ dataset.** NanoString™ nCounter data on the abundance of 237 bone-
521 related mRNA species were used to calculate change in expression ratio between D2 vs

522 D5, D5 vs D10, and D10 vs D28. Expression ratios were analyzed using IPA Upstream
523 Regulator and Canonical Pathways Analysis software and heat maps reflecting the
524 changes in predicted activity during each interval were generated using Morpheus
525 software. **A.** Heat maps depicting changes in selected upstream regulators (rows) with
526 activation z-scores > 2 (red) or < -2 (blue) during at least one phase of differentiation
527 (columns). Upstream regulators were arbitrarily grouped based on their relationship to
528 biological processes or signaling pathways involved in osteoblast differentiation. **B.** Heat
529 maps depicting changes in z-score for selected canonical signaling pathways (rows)
530 during each phase of differentiation (columns). Z-scores were subjected to Euclidean
531 hierarchical clustering in Morpheus to group pathways based on similarity in temporal
532 change.
533
534 We next performed IPA Canonical Pathways Analysis using the NanoString™
535 dataset. The list of signaling pathways represented along with –log(p-value) and
536 activation z-score are shown in S7 Table. Fig. 7B depicts a heat map of predicted changes
537 in activity in selected canonical signaling pathways. Hierarchical clustering was
538 performed to group pathways based on similarities in the change in activity over time.
539 Consistent with the canonical pathways analysis of the microarray dataset (Fig 5),
540 WNT/β-catenin signaling became less active as differentiation progressed, while TGFβ
541 and BMP signaling increased, although the changes in the NanoString™ dataset were
542 more apparent later than in the microarray dataset, between day 10 and day 28.
543 Interleukin signaling was predicted to increase progressively between days 5 and 28, with
544 JAK-STAT signaling showing the activation between days 10 and 28. TNFα/NFκB

545 pathway signaling was likewise predicted to increase in both the NanoString™ and
546 microarray datasets.
547

548 Overview of signaling networks during MC3T3-E1
549 differentiation

550 To test the overall similarity between the NanoString™ and microarray datasets
551 we compared the pathway activity predictions generated from each using the IPA
552 Canonical Pathways molecular activity predictor tool, which graphically depicts the
553 predicted change in pathway activity based on observed changes in upstream and
554 downstream gene expression. S1 Fig shows the WNT/β-catenin pathway comparison
555 using D2 vs D5 expression ratios from each dataset. Since WNT/β-catenin signaling was
556 predicted to decline as differentiation progressed, it would be most active during this
557 interval. Consistent with this, both datasets indicated β-catenin pathway activation in this
558 time frame, as well as inhibition of the negative regulatory TGFβ/TGFβ-activated kinase
559 1 (TAK1)/p38 MAPK/nemo like kinase (NLK) input from the TGFβ receptor pathway
560 that was predicted to be less active early in differentiation. S2 Fig compares IPA
561 predicted changes in activity within the TGFβ/BMP signaling network occurring between
562 days 10 and 28, an interval during which both datasets indicated pathway activation.
563 While the focused Nanostring™ dataset better captured activation of BMP receptor
564 signaling during this phase of differentiation, both datasets predicted net activation of the
565 SMAD2/3 and TAK1/p38 MAPK components of TGFβ signaling. S3 Fig compares the
566 IPA predicted changes in the canonical TNFα/NFκB signaling pathway between days 10
567 and 28 in culture. The TNFα network plays a key role during osteoblast maturation,

568 acting as an inhibitor of osteoblast differentiation and, along with RANKL, promoting
569 osteoclast development [24,25]. Both datasets indicated net activation of NFκB-
570 dependent transcription during MC3T3-E1 maturation related to changes in the
571 expression of TNF family and growth factor ligands and receptors. Both datasets also
572 indicated relative inhibition of interleukin receptor-mediated NFκB activation through
573 TNF receptor-associated factor 6 (TRAF6)/TAK1. S4 Fig illustrates the predicted
574 activation of canonical STAT3 signaling downstream of cytokine and growth factor
575 receptors between days 10 and 28 observed in both the microarray and Nanostring™
576 nCounter datasets. Collectively, the data indicate substantial concordance between the
577 two independent MC3T3-E1 datasets and highlight the evolving changes in WNT/β-
578 catenin, TGFβ/BMP/SMAD, TNFα/RANKL/NFκB, and cytokine/JAK-STAT signaling
579 associated with osteoblast differentiation.

580 To illustrate the temporal evolution of signaling network interaction during
581 MC3T3-E1 cell differentiation, we generated pathway activity predictions for the IPA
582 osteoarthritis canonical pathway, which integrates multiple signal inputs controlling
583 expression of bone-related genes. As the first transcription factor required for osteoblastic
584 differentiation, control of Runx2-dependent transcription is central to the process [17,18].
585 Runx2 activity reflects the input of multiple upstream regulators, notably including BMP
586 receptors signaling via SMAD1/5/8 as well as TGFβ and activin receptors signaling
587 through SMAD2/3. Given that the NanoString™ Code Set was selected to examine bone-
588 related genes, the osteoarthritis network was the most heavily populated canonical
589 pathway in our IPA analysis with a -log(p-value) of 43.3 (S7 Table). Fig 8 shows the
590 pathway activity analysis based on D2 vs D5 expression ratio changes from the

591 NanoString™ nCounter dataset. During this phase, MC3T3-E1 cells are transitioning
592 from log phase growth to growth arrest and initiating the process of differentiation.
593 Based on observed upregulation of Runx2, Sp7 and Sox9 mRNA, Runx2-dependent
594 transcription is predicted to increase from Day 2 to Day 5, associated with increases in
595 mRNA encoding collagen species and alkaline phosphatase. Observed changes in genes
596 encoding Indian Hedgehog (IHH), Patched (PTCH) and β-catenin, as well as TNFα,
597 IL1B, TGFβ and TGFβ receptor 2 (TGFBR2), suggest that the onset of differentiation
598 coincides with upregulation of autocrine ligands and receptors that later come to drive the
599 differentiation process. Notably, TGFβ/BMP signaling is not yet predicted to be active
600 due to relative downregulation of BMP2/9 and SMAD2/3.
601
602 **Fig 8. Changes in canonical signaling pathway activity in MC3T3-E1 cells between**
603 **days 2 and 5.** Expression ratios representing the changing abundance of 237 bone-related
604 mRNA species in MC3T3-E1 cells between days 2 and 5 in culture were used to populate
605 the IPA osteoarthritis pathway network and signaling pathway activation state was
606 assessed using the IPA molecular pathway predictor tool. As indicated in the prediction
607 legend, observed upregulation and downregulation of mRNAs are shown in red and
608 green, respectively, while predicted activation or inhibition of signaling intermediates and
609 pathways are shown in orange and blue.
610
611 Fig 9 depicts the results of an identical analysis performed using the D5 vs D10
612 expression ratio changes from the Nanostring™ nCounter dataset. This phase is
613 associated with osteoblastic differentiation and increased expression of secreted growth

614 factors and matrix components, but relatively little matrix mineralization (Figs 1 and 2).
615 The network analysis suggests that increasing expression of Runx2 and Sp7 is now
616 associated with upregulation of the Runx2-regulated matrix components osteopontin
617 (Spp1) and osteocalcin (Bglap2), and further increases in expression of collagen species
618 and alkaline phosphatase, along with the upstream regulators IHH, β-catenin, TNFα,
619 IL1B, and TGFβ. Increasing expression of BMP2 and BMP9 is now evident, although
620 the molecular pathway predictor still suggests that SMAD1/5/8 and SMAD2/3 signaling
621 is attenuated. Fig 10 depicts predicted changes in signaling pathway activity based on the
622 D10 vs D28 expression ratio changes. This phase is associated with osteoblast
623 maturation, further increases in expression of secreted growth factors and matrix
624 components, and the onset of matrix mineralization. The most notable changes during
625 this interval are the activation of SMAD1/5/8 signaling downstream of BMP receptors
626 and SMAD2/3 signaling from TGFβ receptors. Observed upregulation of the BMP
627 receptors Bmpr1a (ALK3) and Bmpr2 (BMPR2) and the activin-like receptor Acvrl1
628 (ALK1), and SMAD2/3 likely contributes to the prediction of increased pathway activity.
629 Upregulation of PTHrp/PTH1R and FGF2/FGF8 also suggests that GPCR and RTK
630 signaling increase during this interval. Hence the data suggest that during osteoblastic
631 differentiation of MC3T3-E1 cells, activation of β-catenin- and NFκB-mediated
632 pathways occurs prior to the onset of TGFβ/BMP/SMAD-mediated signaling and a
633 general activation of bone developmental signaling pathways.
634
635 **Fig 9. Changes in canonical signaling pathway activity in MC3T3-E1 cells between**
636 **days 5 and 10.** Expression ratios representing the changing abundance of 237 bone-

637 related mRNA species in MC3T3-E1 cells between days 5 and 10 in culture were used to
638 populate the IPA osteoarthritis pathway network and signaling pathway activation state
639 was assessed using the IPA molecular pathway predictor tool. Observed upregulation
640 and downregulation of mRNAs are shown in red and green, respectively, while predicted
641 activation or inhibition of signaling intermediates and pathways are shown in orange and
642 blue.
643
644 **Fig 10. Changes in canonical signaling pathway activity in MC3T3-E1 cells between**
645 **days 10 and 28.** Expression ratios representing the changing abundance of 237 bone-
646 related mRNA species in MC3T3-E1 cells between days 10 and 28 in culture were used
647 to populate the IPA osteoarthritis pathway network and signaling pathway activation state
648 was assessed using the IPA molecular pathway predictor tool. Observed upregulation
649 and downregulation of mRNAs are shown in red and green, respectively, while predicted
650 activation or inhibition of signaling intermediates and pathways are shown in orange and
651 blue.
652

653 # Discussion

654 Complex biological processes like osteoblast development involve the
655 coordinated regulation of multiple intracellular signaling pathways controlling gene
656 expression. Thus, studies focusing on the contribution of any individual growth factor or
657 pathway are invariably incomplete. Developing a more complete picture requires the use
658 of "omics" approaches that capture as much information as possible about changes in
659 intracellular signaling networks in as unbiased a manner as possible. Further

660 complicating matters, bone remodeling *in vivo* is a continuous process wherein
661 osteoblasts at all stages of development, from mesenchymal stem cell precursors to
662 osteocytes are present, along with cells of the osteoclast lineage and other cell types [1,2].
663 As a result, studies performed on bone only provide a "snapshot" of the tissue average
664 transcriptome that represents multiple cell types present in different proportions and
665 differentiations states. In this study, we combined transcriptomics with bioinformatic
666 geneset enrichment analysis to examine the temporal sequence of autocrine and paracrine
667 signaling that regulates the differentiation of MC3T3-E1 cells, a well-characterized
668 model of osteoblast development [7-10]. We employed two independently generated
669 datasets, an "agnostic" DNA microarray dataset intended to provide a global overview of
670 the evolving transcriptome and a "targeted" NanoString™ nCounter dataset focusing on
671 genes involved in specific bone-related pathways. Our data complement other *in vitro*
672 microarray studies of osteoblastic differentiation performed using different cell types, e.g.
673 mesodermal progenitor cells, calvarial osteoblasts, osteocytes, periodontal ligament cells,
674 and embryonic stem cells [21,26-30], or describing the effects of exogenous factors on
675 osteoblast gene expression [31-34].

676 Although osteoblast differentiation *in vivo* is subject to regulation by numerous
677 circulating factors [3], our results underscore the importance of cell autonomous
678 autocrine/paracrine signaling. Key to the process is regulation of Runx2, the most
679 upstream transcription factor in osteoblast differentiation [17,18], which regulates the
680 expression of another critical transcription factor in bone, Sp7 [35]. Runx2 expression in
681 osteoblasts is stimulated by an enhanceosome composed of Dlx5/6, Mef2, Tcf7, β-
682 catenin, Sox5/6, Smad1, and Sp7, and in turn stimulates expression of bone matrix

683 proteins including Spp1, Ibsp, and Bglap2, and autocrine factors including Ihh and Rankl
684 [35,36]. Our data suggest that early MC3T3-E1 differentiation, between Days 2 and 5, is
685 characterized by increasing expression of Runx2, Sp7, and β-catenin and upregulation of
686 IHH, TNFα, and IL1β at a time where TGFβ/BMP/SMAD signaling is still relatively
687 suppressed despite increasing expression of TGFβ and TGFβ receptors. WNT signaling,
688 which cooperates with TGFβ in a positive regulatory loop by inducing Runx2-dependent
689 transcription of TGFβ1 receptor [37,38], appeared most active early and to wane as
690 TGFβ/BMP pathway activity increased, consistent with a role for WNT signaling in the
691 induction of TGFβ signaling. The central role of the TGFβ/BMP axis in regulating
692 mesenchymal stem cell differentiation into cartilage and bone is well established, as both
693 canonical SMAD-dependent and non-canonical p38MAPK signaling downstream of
694 these receptors converge on Runx2 to promote differentiation [19-22]. Moreover, in bone
695 TGFβ/BMP in extensive cross talk with other signaling pathways [4,23]. Of these, the
696 activity of several, including Hedgehog, FGF2, interleukins, TNFα/RANKL and
697 interferon-γ, appeared to increase in parallel with TGFβ/BMP during MC3T3-E1 cell
698 differentiation. Hedgehog signaling, acting through Gli family transcription factors,
699 promotes the expression of BMP2, and IHH has been shown to be required for
700 osteogenesis *in vitro* [39,40]. FGF2 regulates expression of PC1, the primary enzymatic
701 generator of pyrophosphate in mineralizing cells, by direct regulation of Runx2,
702 suggesting that TGFβ/BMP and FGF2 signaling cooperate to promote matrix
703 mineralization later in differentiation [41]. TNFα plays many roles in bone, inhibiting
704 osteoblast differentiation and collagen synthesis (42,43), promoting osteoblast apoptosis
705 (44), while directly stimulating osteoclast formation independent of RANKL signaling

706 through an IL1-dependent mechanism (45,46). Conversely, interferon-γ opposes IL1 and
707 TNFα mediated bone resorption, but produces additive inhibition of bone collagen
708 synthesis (47). Thus our network analysis, demonstrating simultaneous changes in the
709 TGFβ/BMP pathways that favoring osteoblast differentiation and survival, the TNFα
710 pathway that inhibits differentiation and favors apoptosis, and the interferon-γ pathway
711 that inhibits ongoing collagen synthesis, illustrates the complexity of osteoblast
712 development and maturation that occur in the setting of opposing autocrine signaling
713 loops.

714 While gene array technology is a powerful tool for determining the transcriptional
715 basis of changing developmental or pharmacological processes, the resulting datasets are
716 both too complex and too error prone to reliably base conclusions on casual inspection
717 [5,6]. Metabolic pathways analysis overcomes several of these limitations. By basing
718 conclusions on the number and magnitude of expression changes across gene clusters,
719 rather than individual genes, it decreases the probability of false discovery, while
720 simultaneously providing a quantitative measure of the probability of change in a given
721 signaling network. Our analyses illustrate several of the advantages and disadvantages of
722 this approach. The murine Operon V2.0 cDNA arrays employed in this study did not
723 provide genome-wide coverage of changes in mRNA abundance. The NanoString™
724 nCounter system provides information only about rationally chosen transcripts. Hence,
725 some information is missing. Moreover, transcriptomic datasets in general are limited in
726 their ability to discriminate changes in cellular metabolism simply because important
727 pathway components may not be regulated at the transcriptional level, rendering them
728 “invisible” in gene array experiments. Bioinformatic tools, such as IPA, that “infer”

729 changes in upstream pathway activity based on observed changes in network
730 components, provide a means to translate incomplete transcriptomic datasets into a more
731 complete picture of metabolic activity. In our study, we took two independently
732 generated sets of mRNA samples from differentiating MC3T3-E1 cells and employed
733 two different approaches to pathways analysis. Close inspection of the data (S1 and S2
734 Tables) shows that the relatively stringent statistical filter applied to the microarray
735 dataset to define significant change failed to capture factors that were seen in the
736 NanoString™ assay, and conversely, that the targeted NanoString™ Code Set missed
737 significant changes in factors that were detected with the broader coverage provided by
738 the microarrays. It is also noteworthy that some of the interval expression ratios of
739 individual factors were seen to change in opposite directions in the two datasets, such that
740 focusing on the abundance of individual factors might lead to different conclusions. Yet
741 the remarkable degree of similarity in the pathways analysis, which weighs changes
742 across entire networks to predict pathway activation, suggests the approach is both
743 reliable and robust enough to tolerate a substantial amount of "noise" in the raw data.
744 Thus, starting from incomplete datasets, we were able to extract temporal changes in the
745 autocrine/paracrine signaling networks that influence osteoblast differentiation *in vitro*,
746 and find evidence of pathway cross talk at the transcriptional level.
747

748 # Acknowledgements

749 Supported by NIH/NIGMS (R01 GM095497 and R35 GM126955) and the United
750 States Department of Veterans Affairs (I01 BX003188). Some bioinformatic analyses
751 were conducted through the Medical University of South Carolina (MUSC)

752 Proteogenomics Facility that was supported by NIH/NIGMS (P30 GM103342 and P20
753 GM103499) and MUSC's Office of the Vice President for Research. The contents of this
754 article do not represent the views of the Department of Veterans Affairs or the United
755 States Government.

756

757 Author Contributions

758 Conceptualization: DGP, LML. Formal Analysis: LML, JLB. Funding
759 Acquisition: LML. Investigation: MSD, HME-S, DGP, CJH, KMR. Writing: JLB,
760 HME-S, DGP, CJH, LML.

761

762 References

763 1. Raisz LG. Physiology and pathophysiology of bone remodeling. Clin Chem.
764 1999;45:1353-8.
765 2. Hadjidakis DJ, Androulakis II. Bone remodeling. Ann N Y Acad Sci. 2006;1092:385-
766 96.
767 3. Raisz LG. Pathogenesis of osteoporosis: concepts, conflicts, and prospects. J Clin
768 Invest. 2005;115:3318-25.
769 4. Wu M, Chen G, Li YP. TGF-β and BMP signaling in osteoblast, skeletal
770 development, and bone formation, homeostasis and disease. Bone Res. 2016;4:16009.
771 5. Allison DB, Cui X, Page GP, Sabripour M. Microarray data analysis: from disarray to
772 consolidation and consensus. Nat Rev Genet. 2006;7:55-65.
773 6. Maudsley S, Chadwick W, Wang L, Zhou Y, Martin B, Park SS. (2011)

Bioinformatic approaches to metabolic pathways analysis. Methods Mol Biol. 2011;756:99-130.

7. Quarles LD, Wenstrup RJ, Castillo SA, Drezner MK. Aluminum-induced mitogenesis in MC3T3-E1 osteoblasts: potential mechanism underlying neoosteogenesis. Endocrinology. 1991;128:3144-51.

8. Quarles LD, Yohay DA, Lever LW, Caton R, Wenstrup RJ. Distinct proliferative and differentiated stages of murine MC3T3-E1 cells in culture: an in vitro model of osteoblast development. J Bone Miner Res. 1992;7:683-92.

9. Franceschi RT, Iyer BS. Relationship between collagen synthesis and expression of the osteoblast phenotype in MC3T3-E1 cells. J Bone Miner Res 1992;7:235-46.

10. Franceschi RT, Iyer BS, Cui Y. Effects of ascorbic acid on collagen matrix formation and osteoblast differentiation in murine MC3T3-E1 cells. J Bone Miner Res. 1994;9:843-54.

11. Wang D, Christensen K, Chawla K, Xiao G, Krebsbach PH, Franceschi RT. Isolation and characterization of MC3T3-E1 preosteoblast subclones with distinct in vitro and in vivo differentiation/mineralization potential. J Bone Miner Res. 1999;14:893-903.

12. Jones SJ, Gray C, Boyde A, Burnstock G. Purinergic transmitters inhibit bone formation by cultured osteoblasts. Bone. 1997;21:393-9.

13. Wang L, Liu S, Quarles LD, Spurney RF. Targeted overexpression of G protein-coupled receptor kinase-2 in osteoblasts promotes bone loss. Am J Physiol Endocrinol Metab. 2005;288:E826-34.

14. Smyth GK, Speed T. Normalization of cDNA microarray data. Methods. 2003;31: 265-73.

797 15. Geiss GK, Bumgarner RE, Birditt B, Dahl T, Dowidar N, Dunaway DL, et al. Direct
798 multiplexed measurement of gene expression with color-coded probe pairs. *Nature*
799 *Biotechnol*. 2008;26:317–25.
800 16. Kulkarni MM. Digital Multiplexed Gene Expression Analysis Using the NanoString
801 nCounter System. *Curr Protocol Mol Biol*. 2011;25B.10.1–17
802 17. Komori T. Regulation of osteoblast differentiation by Runx2. Adv Exp Med Biol.
803 2010;658:43-9.
804 18. Komori T. Roles of Runx2 in Skeletal Development. Adv Exp Med Biol.
805 2017;962:83-93.
806 19. Noda M, Rodan GA. Type beta transforming growth factor regulates expression of
807 genes encoding bone matrix proteins. Connect Tissue Res. 1989;21:71-5.
808 20. Mundy GR, Bonewald LF. Role of TGF beta in bone remodeling. Ann N Y Acad Sci.
809 1990;593:91-7.
810 21. Qi H, Aguiar DJ, Williams SM, La Pean A, Pan W, Verfaillie CM. Identification of
811 genes responsible for osteoblast differentiation from human mesodermal progenitor
812 cells. Proc Natl Acad Sci U S A. 2003;100:3305-10.
813 22. Augello A, De Bari C. The regulation of differentiation in mesenchymal stem cells.
814 Hum Gene Ther. 2010;21:1226-38.
815 23. Guo X, Wang XF. Signaling cross-talk between TGF-beta/BMP and other pathways.
816 Cell Res. 2009;19:71-88.
817 24. Novack DV. Role of NF-κB in the skeleton. Cell Res. 2011;21:169-82.
818 25. Kearns AE, Khosla S, Kostenuik PJ. Receptor activator of nuclear factor kappaB
819 ligand and osteoprotegerin regulation of bone remodeling in health and disease.

820 Endocr Rev. 2008;29:155-92.

821 26. Granchi D, Ochoa G, Leonardi E, Devescovi V, Baglìo SR, Osaba L, et al. Gene
822 expression patterns related to osteogenic differentiation of bone marrow-derived
823 mesenchymal stem cells during ex vivo expansion. Tissue Eng Part C Methods.
824 2010;16:511-24.

825 27. Kalajzic I, Staal A, Yang WP, Wu Y, Johnson SE, Feyen JH, et al. Expression profile
826 of osteoblast lineage at defined stages of differentiation. J Biol Chem.
827 2005;280:24618-26.

828 28. Dean AK, Harris SE, Kalajzic I, Ruan J. A systems biology approach to the
829 identification and analysis of transcriptional regulatory networks in osteocytes. BMC
830 Bioinformatics. 2009;17;10 Suppl 9:S5.

831 29. Choi HD, Noh WC, Park JW, Lee JM, Suh JY. Analysis of gene expression during
832 mineralization of cultured human periodontal ligament cells. J Periodontal Implant
833 Sci. 2011;41:30-43.

834 30. Bourne S, Polak JM, Hughes SP, Buttery LD. Osteogenic differentiation of mouse
835 embryonic stem cells: differential gene expression analysis by cDNA microarray and
836 purification of osteoblasts by cadherin-11 magnetically activated cell sorting. Tissue
837 Eng. 2004;10:796-806.

838 31. Qin L, Qiu P, Wang L, Li X, Swarthout JT, Soteropoulos P, et al. Gene expression
839 profiles and transcription factors involved in parathyroid hormone signaling in
840 osteoblasts revealed by microarray and bioinformatics. J Biol Chem 2003;278:19723-
841 31.

842 32. Piek E, Sleumer LS, van Someren EP, Heuver L, de Haan JR, de Grijs I, et al. Osteo-
843 transcriptomics of human mesenchymal stem cells: accelerated gene expression and
844 osteoblast differentiation induced by vitamin D reveals c-MYC as an enhancer of
845 BMP2-induced osteogenesis. Bone. 2010;46:613-27.
846 33. Balint E, Lapointe D, Drissi H, van der Meijden C, Young DW, van Wijnen AJ, et al.
847 Phenotype discovery by gene expression profiling: mapping of biological processes
848 linked to BMP-2-mediated osteoblast differentiation. J Cell Biochem. 2003;89:401-
849 26.
850 34. Bernardini C, Saulnier N, Parrilla C, Pola E, Gambotto A, Michetti F, et al. Early
851 transcriptional events during osteogenic differentiation of human bone marrow
852 stromal cells induced by Lim mineralization protein 3. Gene Expr. 2010;15:27-42.
853 35. Komori T. Regulation of osteoblast differentiation by transcription factors. J Cell
854 Biochem. 2006;99:1233-9.
855 36. Kawane T, Komori H, Liu W, Moriishi T, Miyazaki T, Mori M, et al. Dlx5 and Mef2
856 regulate a novel Runx2 enhancer for osteoblast-specific expression. J Bone Min Res.
857 2014;29:1960–9.
858 37. van den Bosch MH, Blom AB, van Lent PL, van Beuningen HM, Blaney Davidson
859 EN, van der Kraan PM, et al. Canonical Wnt signaling skews TGF-β signaling in
860 chondrocytes towards signaling via ALK1 and Smad 1/5/8. Cell Signal. 2014;26:951-
861 8.
862 38. van den Bosch MH, Gleissl TA, Blom AB, van den Berg WB, van Lent PL, van der
863 Kraan PM. Wnts talking with the TGF-β superfamily: WISPers about modulation of
864 osteoarthritis. Rheumatology (Oxford). 2016;55:1536-47.

865 39. Long F, Chung UI, Ohba S, McMahon J, Kronenberg HM, McMahon AP. Ihh
866 signaling is directly required for the osteoblast lineage in the endochondral skeleton.
867 Development. 2004;131:1309-18.
868 40. Zhao M, Qiao M, Harris SE, Chen D, Oyajobi BO, Mundy GR. The zinc finger
869 transcription factor Gli2 mediates bone morphogenetic protein 2 expression in
870 osteoblasts in response to hedgehog signaling. Mol Cell Biol. 2006;26:6197-208.
871 41. Hatch NE, Li Y, Franceschi RT. FGF2 stimulation of the pyrophosphate-generating
872 enzyme, PC-1, in pre-osteoblast cells is mediated by Runx2. J Bone Miner Res.
873 2009;24:652-62.
874 42. Gilbert L, He X, Farmer P, Boden S, Kozlowski M, Rubin J, et al. Inhibition of
875 osteoblast differentiation by tumor necrosis factor-alpha. Endocrinology.
876 2000;141:3956-64.
877 43. Centrella M, McCarthy TL, Canalis E. Tumor necrosis factor-alpha inhibits collagen
878 synthesis and alkaline phosphatase activity independently of its effect on
879 deoxyribonucleic acid synthesis in osteoblast-enriched bone cell cultures.
880 Endocrinology.1988;123:1442-8.
881 44. Jilka RL, Weinstein RS, Bellido T, Parfitt AM, Manolagas SC. Osteoblast
882 programmed cell death (apoptosis): modulation by growth factors and cytokines. J
883 Bone Miner Res. 1998;13:793-802.
884 45. Kobayashi K, Takahashi N, Jimi E, Udagawa N, Takami M, Kotaki S, et al. Tumor
885 necrosis factor alpha stimulates osteoclast differentiation by a mechanism
886 independent of the ODF/RANKL-RANK interaction. J Exp Med. 2000;191:275-86.
887 46. Wei S, Kitaura H, Zhou P, Ross FP, Teitelbaum SL. IL-1 mediates TNF-induced

888 osteoclastogenesis. J Clin Invest. 2005;115:282-90.

889 47. Smith DD, Gowen M, Mundy GR. Effects of interferon-gamma and other cytokines

890 on collagen synthesis in fetal rat bone cultures. Endocrinology. 1987;120:2494-9.

891

892 Supporting Information Captions

893

894 **S1 Fig. Comparison of WNT/β-catenin network activity between Days 2 and 5 of**

895 **MC3T3-E1 cell differentiation predicted from the microarray and NanoString™**

896 **datasets.** Observed Day 2 to Day 5 changes in expression ratios were used to predict

897 WNT/β-catenin pathway activity using the IPA molecular activity predictor tool. **A.**

898 Pathway activity prediction based on the microarray dataset. **B.** Pathway activity based

899 on the NanoString™ dataset. Observed increases (*red*) and decreases (*green*) in mRNA

900 abundance are indicated, as are predicted activation (*orange*) and inhibition (*blue*) of

901 downstream targets.

902

903 **S2 Fig. Comparison of TGFβ/BMP network activity between Days 10 and 28 of**

904 **MC3T3-E1 cell differentiation predicted from the microarray and NanoString™**

905 **datasets.** Observed Day 10 to Day 28 changes in expression ratios were used to predict

906 TGFβ/BMP pathway activity using the IPA molecular activity predictor tool. **A.**

907 Pathway activity prediction based on the microarray dataset. **B.** Pathway activity based

908 on the NanoString™ dataset. Observed increases (*red*) and decreases (*green*) in mRNA

909 abundance are indicated, as are predicted activation (*orange*) and inhibition (*blue*) of

910 downstream targets.

S3 Fig. Comparison of NFκB network activity between Days 10 and 28 of MC3T3-E1 cell differentiation predicted from the microarray and NanoString™ datasets. Observed Day 10 to Day 28 changes in expression ratios were used to predict NFκB pathway activity using the IPA molecular activity predictor tool. **A.** Pathway activity prediction based on the microarray dataset. **B.** Pathway activity based on the NanoString™ dataset. Observed increases (*red*) and decreases (*green*) in mRNA abundance are indicated, as are predicted activation (*orange*) and inhibition (*blue*) of downstream targets.

S4 Fig. Comparison of STAT3 network activity between Days 10 and 28 of MC3T3-E1 cell differentiation predicted from the microarray and NanoString™ datasets. Observed Day 10 to Day 28 changes in expression ratios were used to predict STAT3 pathway activity using the IPA molecular activity predictor tool. **A.** Pathway activity prediction based on the microarray dataset. **B.** Pathway activity based on the NanoString™ dataset. Observed increases (*red*) and decreases (*green*) in mRNA abundance are indicated, as are predicted activation (*orange*) and inhibition (*blue*) of downstream targets.

S1 Table. NanoString™ nCounter expression data for 237 bone-related transcripts. Gene symbol, accession number, annotation, NanoString™ probe ID, and mRNA abundance data are shown for triplicate determinations at each of four time points.

S2 Table. Operon V2.0 microarray expression data for 1005 significantly-regulated transcripts. Gene symbol, accession number, gene name, mRNA abundance data, and z-standardized expression values are shown for triplicate determinations at each of four time points.

S3 Table. IPA Disease or Function analysis of significantly-regulated transcripts identified by microarray. Disease or function annotation, -log(p value), activation z-score, number and name of pathway molecules are shown for all functions with activation z-score >1 or <-1 in the D2 vs D5, D5 vs D10, and D10 vs D28 pairwise comparisons.

S4 Table. IPA Upstream Regulator analysis of significantly-regulated transcripts identified by microarray. Gene symbol and activation z-score are shown for all upstream regulators with activation z-score >2 or <-2 in the D2 vs D5, D5 vs D10, and D10 vs D28 pairwise comparisons.

S5 Table. IPA Canonical Pathways analysis of significantly-regulated transcripts identified by microarray. Canonical Pathway name, -log(pvalue), activation z-score, and observed pathway molecules are shown for predicted regulated pathways in the D2 vs D5, D5 vs D10, and D10 vs D28 pairwise comparisons.

S6 Table. IPA Upstream Regulator analysis of the NanoString dataset of bone-related genes. Gene symbol and activation z-score are shown for all upstream regulators

956 with activation z-score >2 or <-2 in the D2 vs D5, D5 vs D10, and D10 vs D28 pairwise
957 comparisons.
958
959 **S7 Table. IPA Canonical Pathways analysis of the NanoString dataset of bone-**
960 **related genes.** Canonical Pathway name, -log(pvalue), activation z-score, and observed
961 pathway molecules are shown for predicted regulated pathways in the D2 vs D5, D5 vs
962 D10, and D10 vs D28 pairwise comparisons.

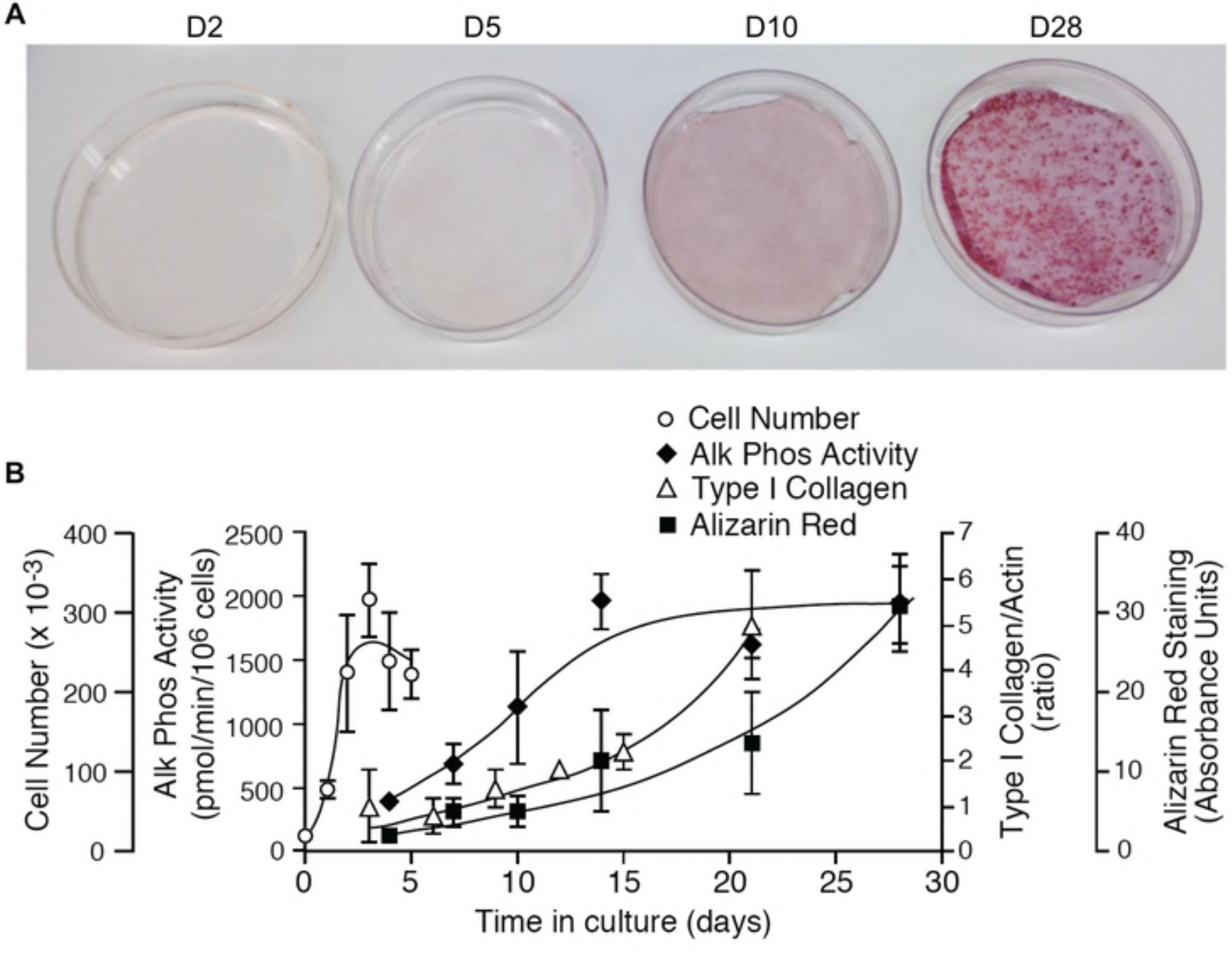
A
D2
D5
D10
D28
B
Cell Number
Alk Phos Activity
Type I Collagen
Alizarin Red
Cell Number (x 10-3)
Alk Phos Activity (pmol/min/10^6 cells)
Type I Collagen/Actin (ratio)
Alizarin Red Staining (Absorbance Units)
Time in culture (days)
0
5
10
15
20
25
30
100
200
300
400
500
1000
1500
2000
2500
1
2
3
4
6
7
10
20
30
40

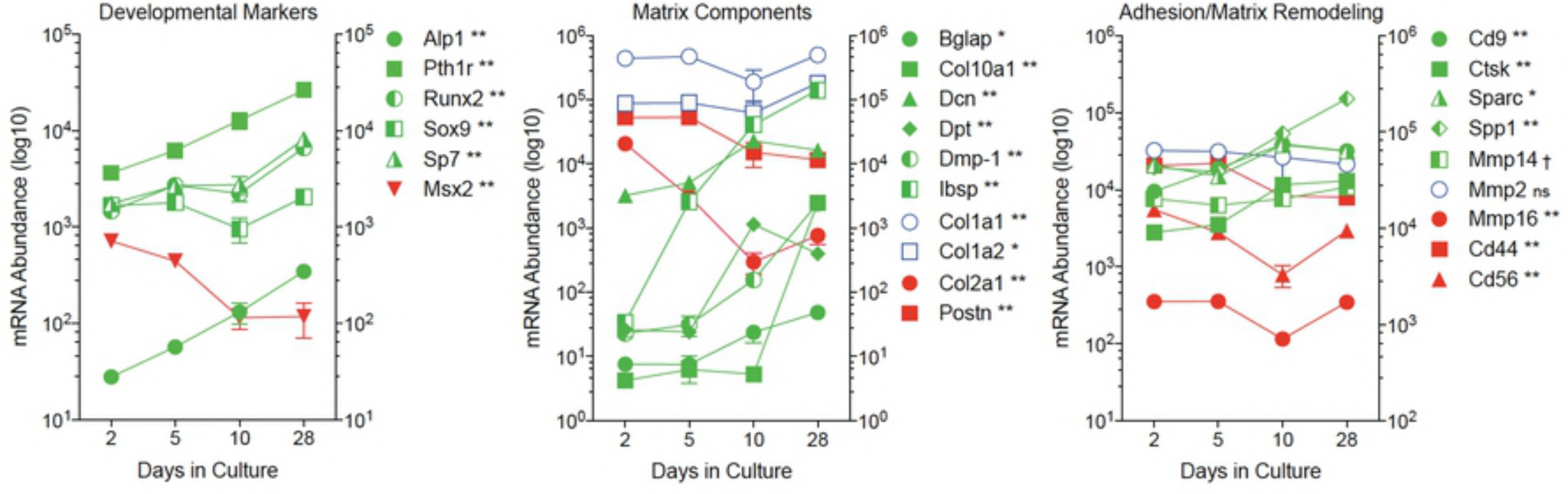
Developmental Markers
mRNA Abundance (log10)
Days in Culture
2
5
10
28
Alp1 **
Pth1r **
Runx2 **
Sox9 **
Sp7 **
Msx2 **
Matrix Components
Bglap *
Col10a1 **
Dcn **
Dpt **
Dmp-1 **
Ibsp **
Col1a1 **
Col1a2 *
Col2a1 **
Postn **
Adhesion/Matrix Remodeling
Cd9 **
Ctsk **
Sparc *
Spp1 **
Mmp14 †
Mmp2 ns
Mmp16 **
Cd44 **
Cd56 **

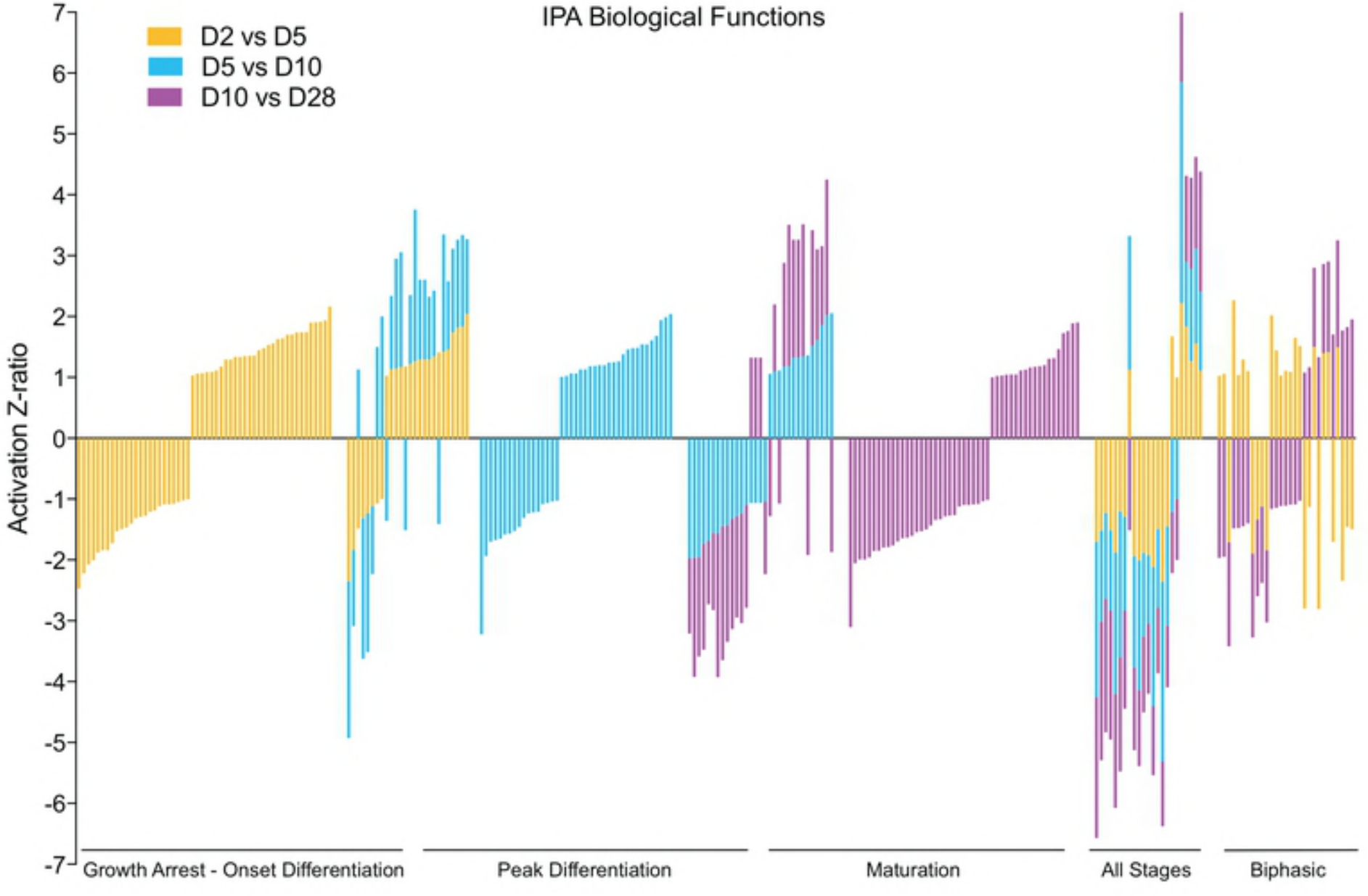
IPA Biological Functions
D2 vs D5
D5 vs D10
D10 vs D28
Activation Z-ratio
7
6
5
4
3
2
1
0
-1
-2
-3
-4
-5
-6
-7
Growth Arrest - Onset Differentiation
Peak Differentiation
Maturation
All Stages
Biphasic

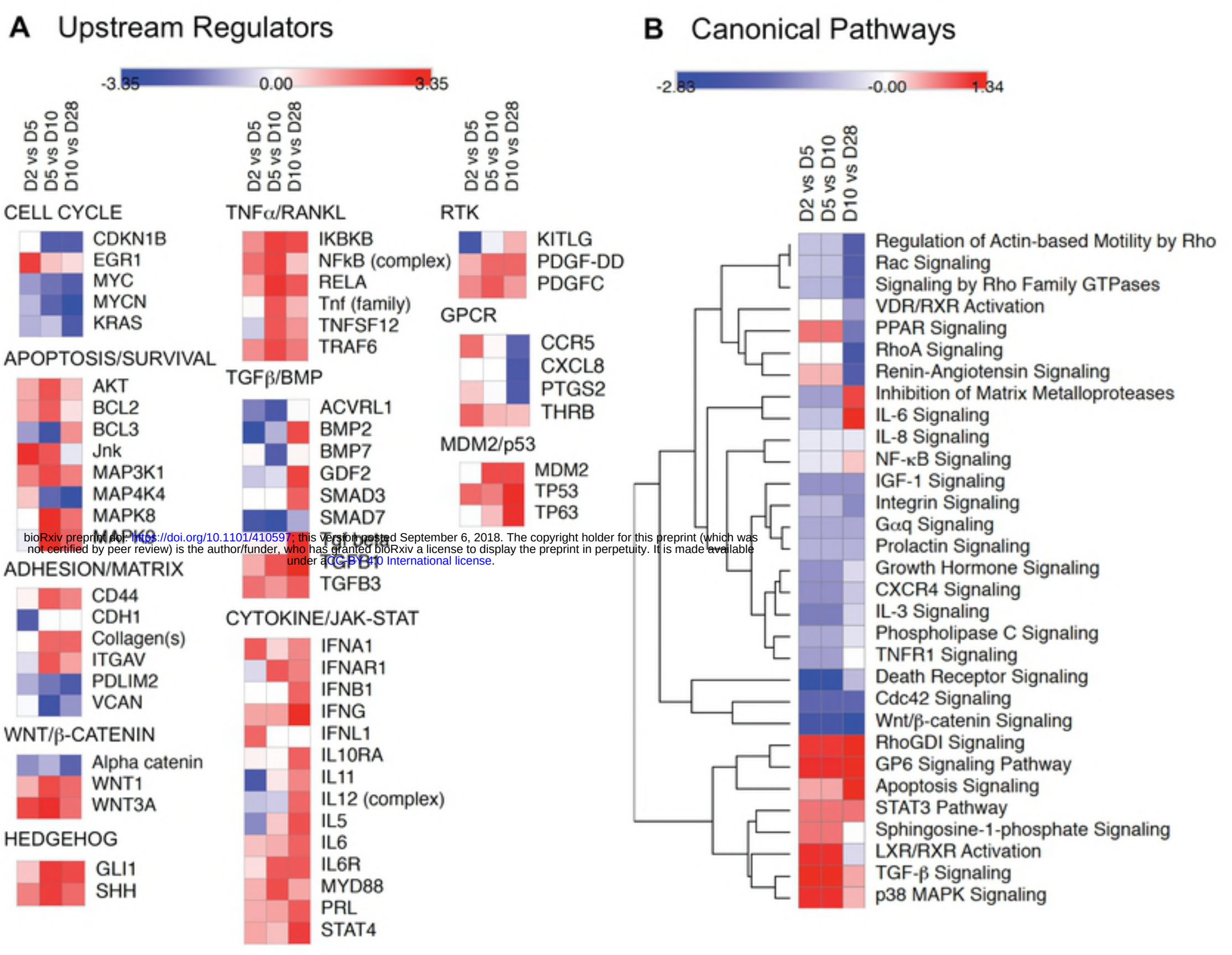

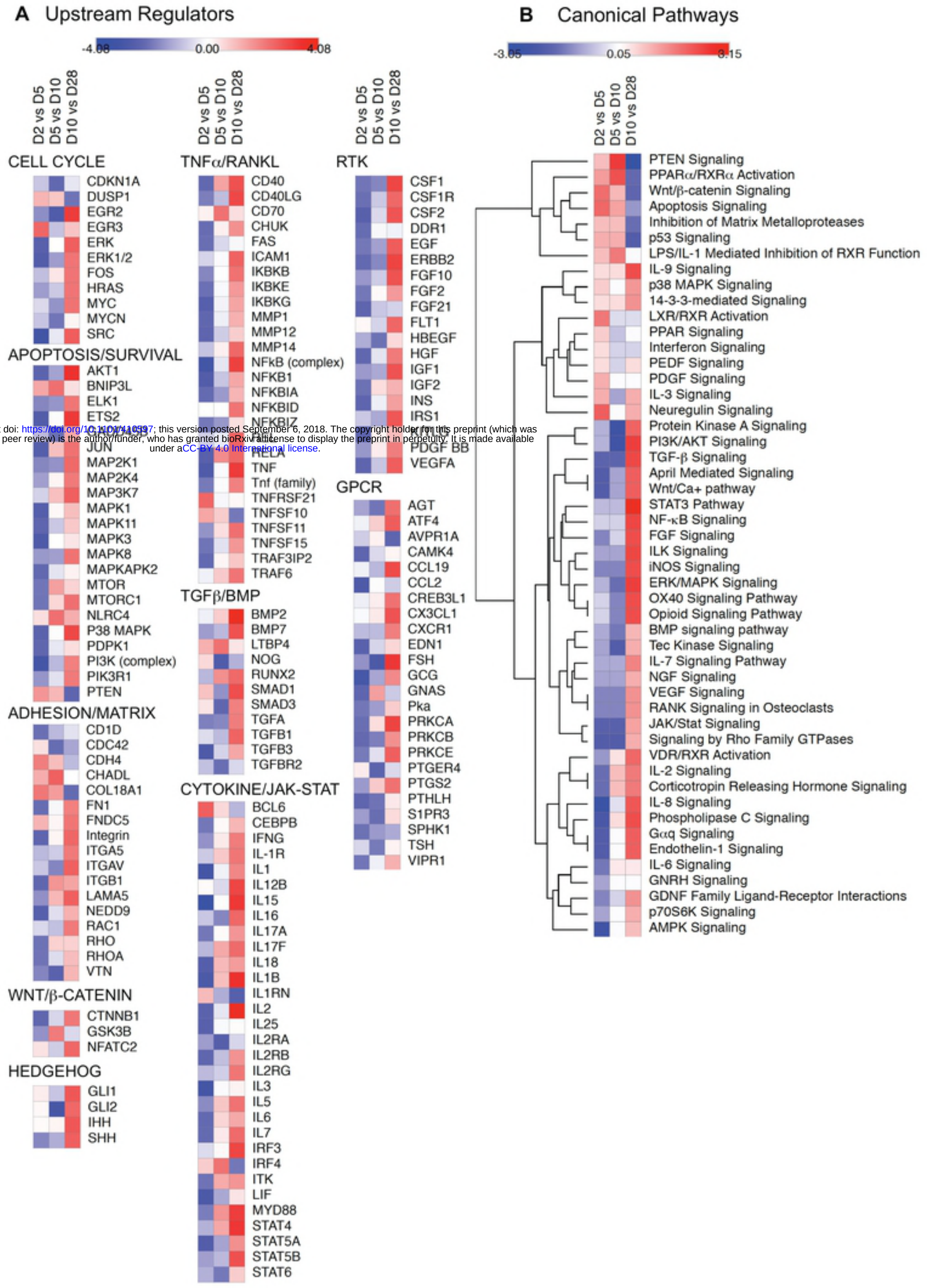

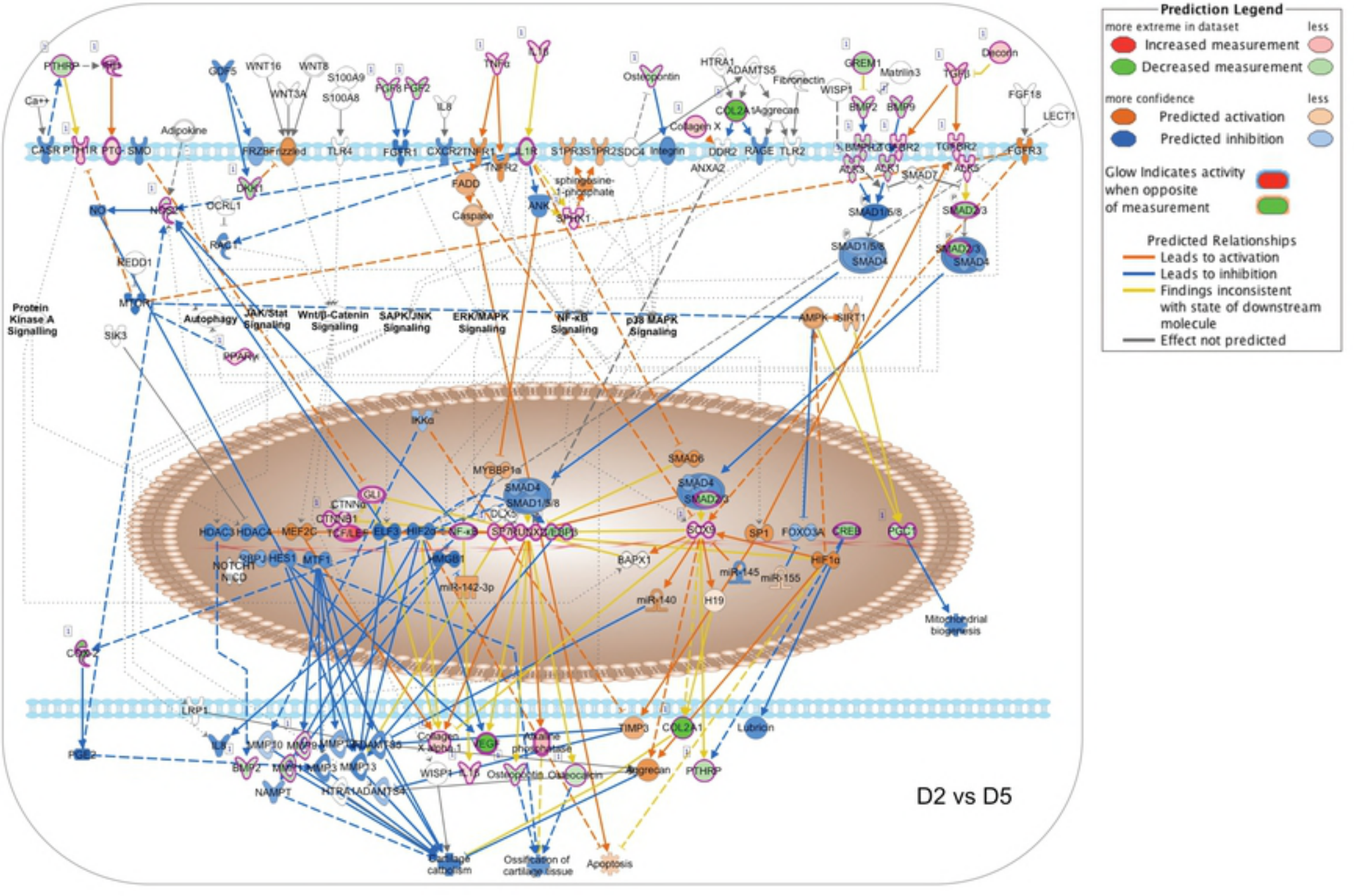
Prediction Legend
more extreme in dataset
less
Increased measurement
Decreased measurement
more confidence
less
Predicted activation
Predicted inhibition
Glow Indicates activity when opposite of measurement
Predicted Relationships
Leads to activation
Leads to inhibition
Findings inconsistent with state of downstream molecule
Effect not predicted
D2 vs D5
Protein Kinase A Signalling
Autophagy
JAK/Stat Signaling
Wnt/β-Catenin Signaling
SAPK/JNK Signaling
ERK/MAPK Signaling
NF-κB Signaling
p38 MAPK Signaling
AMPK
SIRT1
Mitochondrial biogenesis
Cartilage catabolism
Ossification of cartilage tissue
Apoptosis

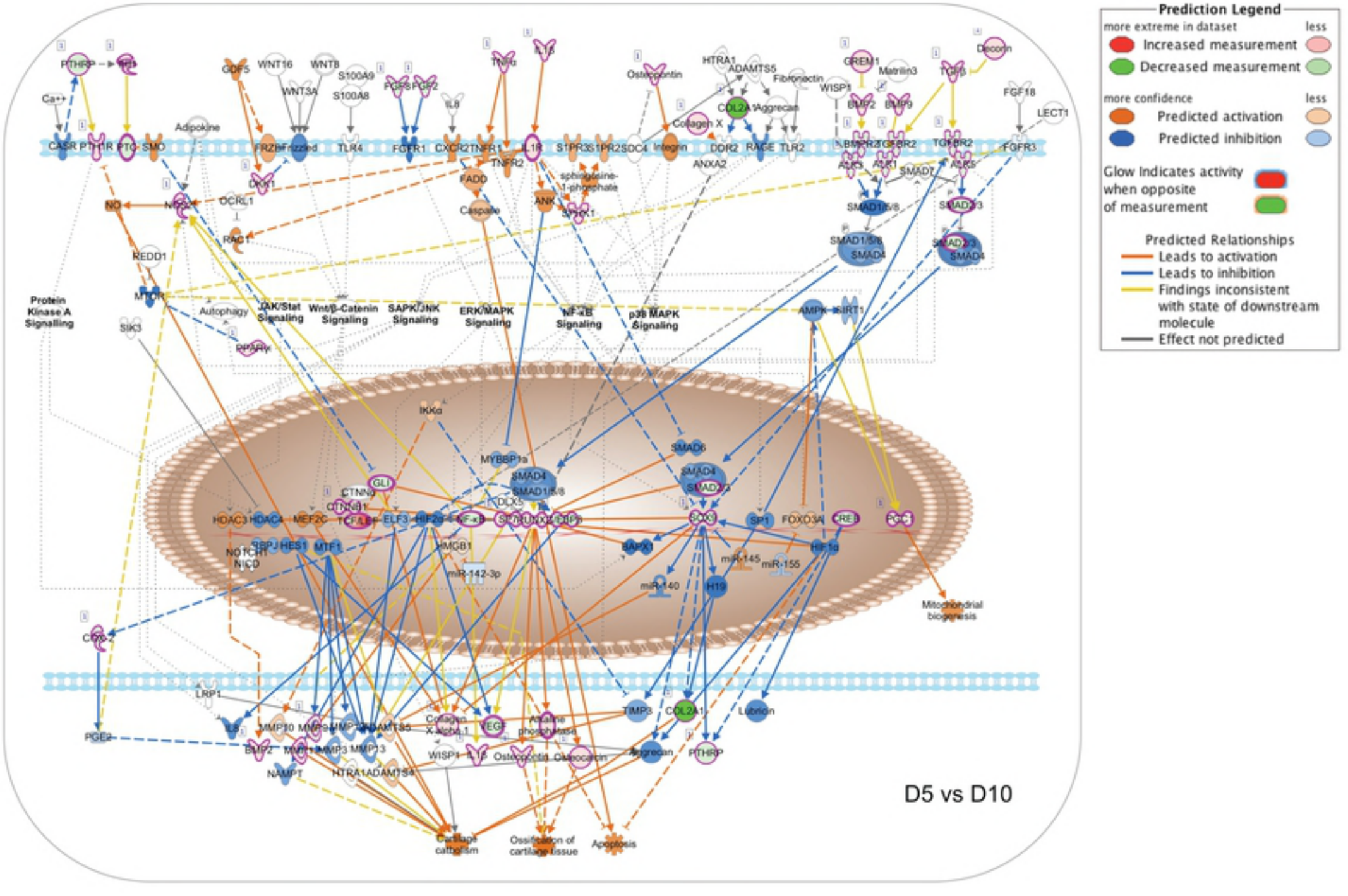
Prediction Legend
more extreme in dataset
less
Increased measurement
Decreased measurement
more confidence
less
Predicted activation
Predicted inhibition
Glow Indicates activity when opposite of measurement
Predicted Relationships
Leads to activation
Leads to inhibition
Findings inconsistent with state of downstream molecule
Effect not predicted
D5 vs D10
Protein Kinase A Signalling
JAK/Stat Signaling
Wnt/β-Catenin Signaling
SAPK/JNK Signaling
ERK/MAPK Signaling
NF-κB Signaling
p38 MAPK Signaling
AMPK
SIRT1
Autophagy
PPARγ
SIK3
REDD1
MTOR
NO
NOS3
OCRL1
RAC1
DKK1
FRZB
Frizzled
TLR4
FGFR1
CXCR2
TNFR1
IL1R
S1PR3
S1PR2
SDC4
Integrin
DDR2
RAGE
TLR2
ANXA2
FADD
Caspase
ANK
SPHK1
sphingosine-1-phosphate
ACVRL1
ALK1
ALK5
SMAD7
SMAD1/5/8
SMAD2/3
SMAD4
TGFBR2
BMPR2
BMP2
BMP9
GREM1
Matrilin3
Decorin
FGF18
LECT1
WISP1
Fibronectin
HTRA1
ADAMTS5
COL2A1
Aggrecan
Collagen X
Osteocrontin
Adipokine
CASR
PTH1R
PTC
SMO
GDF5
WNT16
WNT5B
WNT3A
S100A9
S100A8
FGF2
IL8
TNFα
IL1β
Ca++
PTHRP
IKKα
MYBBP1a
GLI
CTNNB1
CTNND1
DLX5
HDAC3
HDAC4
MEF2C
TCF7L2
ELF3
HIF2α
NF-κB
SP1
FOXO3A
CREB
PGC1
NOTCH1
NICD
RBPJ
HES1
MTF1
HMGB1
miR-142-3p
BAPX1
miR-140
miR-145
miR-155
H19
HIF1α
Mitochondrial biogenesis
CCL2
PGE2
LRP1
IL8
MMP10
MMP3
MMP13
ADAMTS5
BMP2
NAMPT
HTRA1
ADAMTS4
Collagen X
Alpha-1
VEGF
Alkaline phosphatase
WISP1
IL1β
Osteocrontin
Osteocalcin
TIMP3
COL2A1
Aggrecan
PTHRP
Lubricin
Cartilage catbolism
Ossification of cartilage tissue
Apoptosis

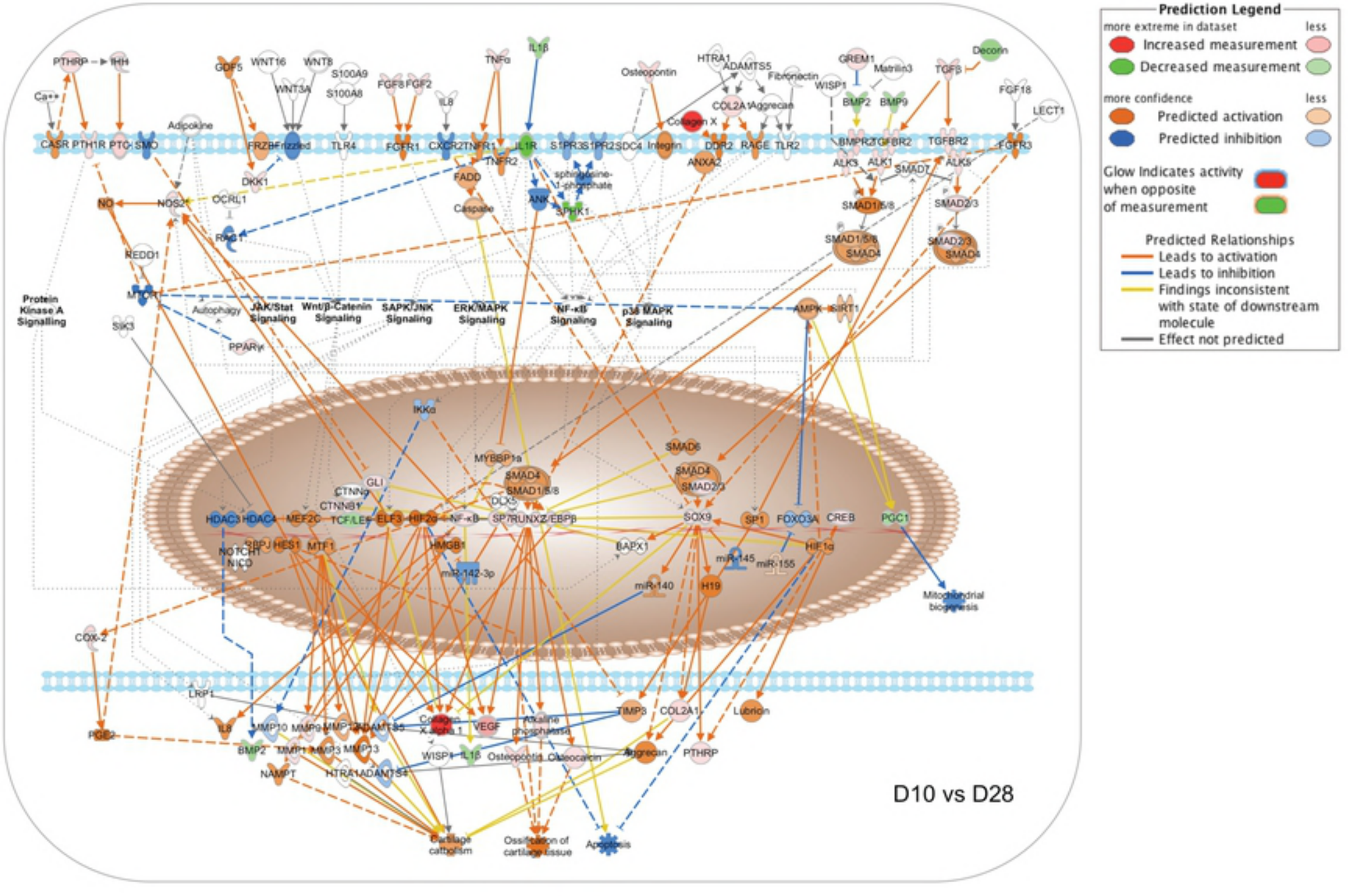
Prediction Legend
more extreme in dataset
less
Increased measurement
Decreased measurement
more confidence
less
Predicted activation
Predicted inhibition
Glow Indicates activity when opposite of measurement
Predicted Relationships
Leads to activation
Leads to inhibition
Findings inconsistent with state of downstream molecule
Effect not predicted
Protein Kinase A Signalling
Autophagy
JAK/Stat Signaling
Wnt/β-Catenin Signaling
SAPK/JNK Signaling
ERK/MAPK Signaling
NF-κB Signaling
p38 MAPK Signaling
AMPK
SIRT1
PTHrP
IHH
Ca++
GDF5
WNT16
WNT5B
WNT3A
S100A9
S100A8
FGF8
FGF2
IL8
TNFα
IL1β
Osteopontin
HTRA1
ADAMTS5
Fibronectin
COL2A1
Aggrecan
GREM1
Matrilin3
WISP1
BMP2
BMP9
TGFβ
Decorin
FGF18
LECT1
CASR
PTH1R
PTC
SMO
Adipokine
FRZB
Frizzled
TLR4
FGFR1
CXCR2
TNFR1
IL1R
S1PR3
S1PR2
SDC4
Integrin
Collagen X
DDR2
RAGE
TLR2
ANXA2
BMPR2
TGFBR2
FGFR3
ALK3
ALK1
SMAD7
ALK5
DKK1
FADD
TNFR2
sphingosine-1-phosphate
ANK
SPHK1
Caspase
NO
NOS2
OCRL1
RAC1
SMAD1/5/8
SMAD2/3
SMAD4
REDD1
MTOR
SIK3
PPARγ
IKKα
MYBBP1a
SMAD6
GLI
CTNNB1
DLX5
HDAC3
HDAC4
MEF2C
TCF/LEF
ELF3
HIF2α
NF-κB
SP7/RUNX2
EBPβ
SOX9
SP1
FOXO3A
CREB
PGC1
RBPJ
HES1
MTF1
NOTCH1
NICD
HMGB1
BAPX1
HIF1α
miR-142-3p
miR-145
miR-155
miR-140
H19
Mitochondrial biogenesis
COX-2
PGE2
LRP1
IL8
MMP10
MMP9
MMP13
ADAMTS5
Collagen X alpha 1
VEGF
Alkaline phosphatase
TIMP3
COL2A1
Lubricin
BMP2
MMP1
MMP3
MMP13
WISP1
IL1β
Osteopontin
Osteocalcin
Aggrecan
PTHrP
NAMPT
HTRA1
ADAMTS4
Cartilage catbolism
Ossification of cartilage tissue
Apoptosis
D10 vs D28